UNIVERSITY OF OKLAHOMA

GRADUATE COLLEGE

SPURIOUS SUPPRESSION TECHNIQUES IN INTEGRATED AND EMBEDDED MICROWAVE COMPONENTS

A THESIS

SUBMITTED TO THE GRADUATE FACULTY

in partial fulfillment of the requirements for the

Degree of

MASTER OF SCIENCE

By

GRANT KARBER

Norman, Oklahoma

2021

SPURIOUS SUPPRESSION TECHNIQUES IN INTEGRATED AND EMBEDDED MICROWAVE COMPONENTS

A THESIS APPROVED FOR THE
SCHOOL OF ELECTRICAL AND COMPUTER ENGINEERING

BY THE COMMITTEE CONSISTING OF

Dr. Jay McDaniel, Chair

Dr. Hjalti Sigmarsson

Dr. Caleb Fulton

Acknowledgments

I would like to greatly thank my advisors, Dr. Jay McDaniel and Dr. Hjalti Sigmarsson, for their mentorship and support. During my time at the Advanced Radar Research Center (ARRC), they have challenged me to think creatively and critically as a student and a researcher. Their advice was invaluable to me as I explored different techniques of spurious suppression and carved out a path to a solution. Their suggestions and feedback have enhanced my technical and soft skills, and they have shaped me into a better engineer. This work simply could not have happened without their guidance and encouragement.

I would also like to thank Dr. Caleb Fulton and Dr. Jorge Salazar for giving me the opportunity to be a teacher assistant for them during my time in graduate school. Helping teach Electromagnetic Fields I gave me a greater understanding of EM waves that I could directly apply to my research. It was a pleasure assisting them and helping students learn about electromagnetics.

I was fortunate to have many great colleagues at the ARRC, many of whom have helped me along the way. I would like to thank Gokhan Ariturk for teaching me how to use the laser machine and Eric Wells for showing me the ProConduct process. I very much appreciated Rylie Mattingly for helping me resolve many software issues I experienced while simulating my designs. Thanks to Russell Kenney for encouraging my interest in research and for the friendly advice he has given me over the years. I wish them all well in their future careers and academic studies.

Lastly, I would like to thank my parents, Doug and Cristie Karber, and my siblings, Juliana and Emma Karber, for their constant love and support. I would not be in the same place in life without their sacrifices and investment in me. I cannot thank them enough.

Table of Contents

List of Tables **ix**

List of Figures **x**

Abstract **xiii**

1 Introduction **1**

1.1 Motivation 1

1.2 Spurious Suppression 3

1.3 SISL Technology 5

1.4 Research Objectives 7

1.5 Thesis Outline 7

2 SISL Filter Design **9**

2.1 Lumped Filter 10

2.1.1 Filter Prototypes and Transformation 10

2.1.2 Simulated Results 11

2.2 Effective Permittivity of SISL Cavity 13

2.3 Distributed Filter 14

2.3.1 Distributed Transformations 14

2.3.2 Simulated Results 16

2.4 HFSS Filter Model 18

2.4.1 SISL Cavity Model 19

2.4.2 Shrinking the SISL Cavity 21
2.4.3 CPWG-SISL Transition 22
2.4.4 Full Filter Model 24
2.4.5 Simulated Results 24
2.4.6 Measured Results 25
2.5 Modal Analysis of Spurious Responses 26

3 Aperture Coupled SIW Resonators 28
3.1 Cavity Resonator Theory 29
3.2 Aperture Coupling Theory 30
3.3 Design Parameters 31
3.4 Design Steps 34
3.5 Simulated Results 35
3.6 Conclusions 38

4 Integrated Resonant Ground Structures 39
4.1 Defected Ground Structure Theory 39
4.2 Resonant Ground Structure Theory 42
4.3 Design Parameters 43
4.4 Design Steps 45
4.5 Simulated Results 47
4.6 Conclusions 49

5 Results and Analysis 50
5.1 Fabrication 50
5.2 Measured Results 51
5.3 Analysis 55

6 Conclusion 56
6.1 Summary 56

6.2 Scientific Impact 57
6.3 Future Work 58
6.3.1 Absorptive Filter 58
6.3.2 RGS Design Equations 59
6.3.3 Coplanar RGSs 60
6.3.4 Absorptive Vias 60

References **61**

A SISL Filter Fabrication Process **66**
A.1 Detailed Fabrication Process 67
A.1.1 Laser Etch Board Designs 68
A.1.2 ProConduct Process 68
A.1.3 Laser Cut Board Designs 69
A.1.4 Assemble Layers 69

B List of Acronyms and Abbreviations **71**

List of Tables

1.1 Comparison of Spurious Suppression Techniques. 5

2.1 Filter prototype values for Generalized Chebyshev 10
2.2 Transformed values for Generalized Chebyshev 11
2.3 Dimensions of MWO Distributed Filter 16
2.4 Dimensions of HFSS Distributed Filter 18
2.5 Dimensions of CPWG-SISL Transition 23

4.1 Metrics of Varied Permittivity 44
4.2 Metrics of Varied Thickness 45

List of Figures

1.1 Examples of Integrated Microwave Assemblies (IMAs) [3] 2
1.2 Frequency-Normalized Amplitude Response of Lumped (Top) and Distributed (Bottom) Low-Pass Filter [6] 3
1.3 Cross section of Suspended Stripline [18] 6
1.4 PCB Stack-up of SISL Thru-line [19] 6

2.1 Schematic of Filter Prototypes 10
2.2 Schematic of Lumped-Element Generalized Chebyshev Filter 11
2.3 S-Parameters of Lumped-Element Generalized Chebyshev Filter . . 12
2.4 S_{21} Phase of Lumped-Element Generalized Chebyshev Filter 12
2.5 HFSS Model for Eigenmode Simulation 13
2.6 MWO Layout of Distributed Generalized Chebyshev Filter 16
2.7 S-Parameters of Lumped and Distributed Generalized Chebyshev Filters 17
2.8 Periodic S_{21} of Distributed Generalized Chebyshev Filter 17
2.9 HFSS Layout of Distributed Generalized Chebyshev Filter 18
2.10 Exploded View of SISL Cavity Model 19
2.11 S-Parameters of MWO and HFSS Cavity Filters 20
2.12 Electric Fields of Cavity Resonance at 9.66 GHz 20
2.13 Exploded View of Shrunk SISL Cavity Model 21
2.14 S-Parameters of MWO and HFSS Filters for Shrunk Cavity 22
2.15 CPWG-SISL Transition 23

2.16 Exploded View of SISL Stackup 24
2.17 S-Parameters of MWO and HFSS Filters 25
2.18 S-Parameters of Simulated and Measured Filters 26
2.19 Modal Analysis at 8 GHz 27
2.20 Modal Analysis at 10 GHz 27

3.1 Substrate Integrated Waveguide [32] 29
3.2 Magnitude of Electric Field in SIW 30
3.3 SIW Cavity Model 31
3.4 Square and Circular SIW 32
3.5 Dimensions of aperture: angle θ and thickness t 33
3.6 S_{21} of Varied Arc Angle (θ) 33
3.7 S_{21} for Varied Thickness (t) 34
3.8 Aperture coupled SIW Resonator Design Flow Graph 35
3.9 Filter Cavity SIW Model 36
3.10 Cavity Filter with SIW at 8 GHz 36
3.11 Cavity Filter with SIW at 8 GHz 37
3.12 Cavity Filter with SIW at 8 GHz 38

4.1 Barbell DGS in Microstrip Line [37] 40
4.2 Ideal DGS Model 41
4.3 Isometric View (a) and Side View (b) of Barbell RGS in Microstrip [38] 42
4.4 RGS Cavity Model 43
4.5 Substrate Dimensions of the RGS 43
4.6 Transmission Behaviour of Varied Permittivity in RGS Substrate . . 44
4.7 Transmission Behaviour of Varied Thickness in RGS Substrate . . . 45
4.8 RGS Design Flow Graph 46
4.9 RGS Cavity Filter Model 47

4.10 Cavity Filter with RGS at 8 GHz 48
4.11 Cavity Filter with RGS at 10 GHz 48
4.12 Cavity Filter with RGS at 9.14 GHz 49

5.1 Fabricated SISL Filter 51
5.2 S-Parameters of RGSs in SISL Thru-line 52
5.3 S-Parameters of RGSs in SISL Thru-line 52
5.4 Responses of 8 GHz RGS in SISL Filter 53
5.5 Responses of 10 GHz RGS in SISL Filter 54
5.6 Responses of 8 and 10 GHz RGS in SISL Filter 54

6.1 Absorptive Filter Response in SISL 59

A.1 Fabrication Process of SISL Filter 70

Abstract

To increase bandwidth and mitigate interference in a crowded electromagnetic spectrum, future microwave systems will move to higher operating frequencies. Because lumped elements perform poorly at high frequencies, designers use distributed elements for most microwave circuits and systems. Traditional distributed elements such as waveguides and coaxial cables are bulky, heavy, and costly, making them unsuitable for applications that require reduced size, weight, power, and cost (SWaP-C). Consequently, these distributed technologies have been planarized and integrated into printed circuit boards (PCBs) and embedded in inner layers to save board space and costs. However, these new distributed technologies often create higher-order modes (HOMs), unintentional resonances, and periodic effects that degrade out-of-band performance. If these issues go unaddressed, microwave systems can experience data corruption, interference, or component damage.

This thesis seeks to improve the performance of microwave components by exploring techniques to suppress spurious signals and responses. The proposed techniques suppress the periodicity of commensurate lines and dampen unintentional resonances. This work produces a design of an embedded, low SWaP-C, 3-GHz, low-pass filter with spurious response suppression of greater than 10 dB up to 14.5 GHz, compared to the original design with spurious responses starting at 8 GHz. The spurious suppression techniques demonstrated in this work have the potential to enhance the performance of many different integrated microwave components.

Chapter 1

Introduction

1.1 Motivation

Next generation radio frequency (RF) and microwave systems need to meet the increasing demands for low size, weight, power, and cost (SWaP-C) as platforms become smaller in form factor and higher in production. Previous systems are unsuitable for new platforms because of their heavy payload, high power consumption, and high costs. To meet SWaP-C demands, integrated microwave assemblies (IMAs) have been developed for many different microwave systems (see Fig. 1.1). Because of their low SWaP-C, IMAs are used on unmanned aerial vehicles (UAVs) for remote sensing, navigation, radar, and many other applications [1]. The design of high-performance integrated components is essential for compact IMAs. More recently, integrated microwave technology advancements have led to multi-layer millimeter-wave multi-chip modules (MCMs) that produce highly compact systems with integrated circuits on outer layers and passive components such as antennas and filters embedded in inner layers [2]. Embedded components give designers more flexibility in multi-layer board designs, as well as saving board space. With current trends in technology, new integrated and embedded components need to be developed to deliver superior performance for integrated microwave systems.

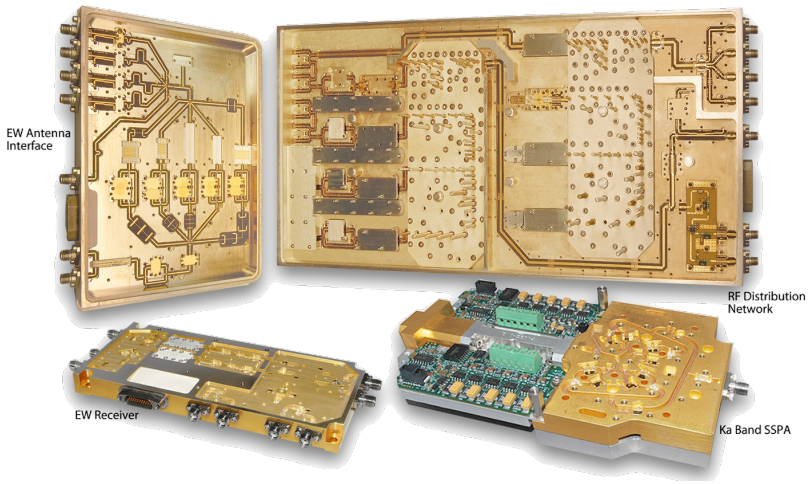

Figure 1.1: Examples of Integrated Microwave Assemblies (IMAs) [3]

Compared to lumped components, distributed components use transmission lines and waveguides and have unique performance degradation. This performance degradation is due to higher-order modes (HOMs), unintentional resonances, and periodicity. Electromagnetic waves of many different field distributions called modes can propagate in distributed components. Most distributed components operate using the dominant mode of propagation, and higher-order modes start to propagate at higher, out-of-band frequencies. HOMs lead to excess power loss and undesired coupling in distributed components and can be found in waveguides and stripline [4]. Unintentional resonances occur when the geometry of a distributed component creates an unwanted standing wave at a select resonant frequency. At the resonant frequency, the distributed component can exhibit undesirable behavior outside its desired operating frequency. Unintentional resonances are often the byproduct of shielding that contains fields to prevent radiation and interference with other components or systems [5]. Periodicity is a phenomenon where the response of a distributed component recurs at regular intervals of frequency (see Fig. 1.2). Periodicity degrades the stopband performance of distributed components [4].

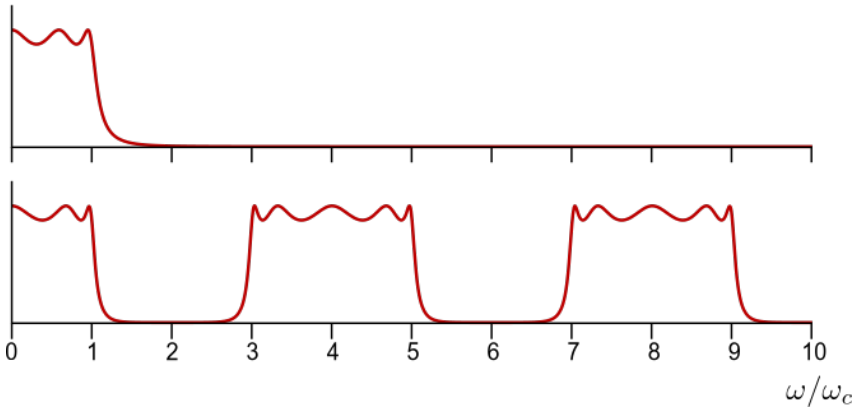

Figure 1.2: Frequency-Normalized Amplitude Response of Lumped (Top) and Distributed (Bottom) Low-Pass Filter [6]

Components with significant HOMs, unintentional resonances, or periodicity affect system performance by passing spurious signals into the system. For reference, the term spurious or spur is often applied to unwanted signals in a system. In a microwave transmit (Tx) chain, spurious signals waste transmit power and cause interference in an already crowded electromagnetic spectrum. In a microwave receive (Rx) chain, high-power spurious signals overload the system, corrupt data, and damage sensitive components. For these reasons, it is critical to find ways to eliminate or suppress spurs in systems.

1.2 Spurious Suppression

Spurious suppression is an area of research that suppresses spurious emission or transmission of microwave components caused by HOMs, unintentional resonances, periodicity, or harmonics [4]. Efforts for spurious suppression are found in many different microwave components, including antennas [7], amplifiers [8], mixers [9], rat race couplers [10], and filters [11, 12]. Recent research has suppressed the spurious responses of microwave components by changing the geometry of ele-

ments. In [11], a coupled-line microstrip bandpass filter has been miniaturized using capacitive terminations, and the miniaturization suppresses the second and third harmonic frequencies of the filter. Changing the inherent geometry does miniaturize the component and suppress spurious responses, but it comes at the cost of increased design complexity.

Another technique of suppressing spurious signals is to insert defects in the ground plane. In [13], a coupled-line microstrip bandpass filter has been reduced in size, and its second, third, and fourth harmonics have been suppressed using defected ground structures (DGSs). Creating defects in the ground plane is another effective method for miniaturization and spurious response suppression, but it again comes at a cost. DGSs radiate and can cause electromagnetic compatibility (EMC) issues within a microwave system, and electromagnetic interference (EMI) issues with other microwave systems [14]. DGSs also induce effective inductances and capacitances on transmission lines that if unaccounted for can change the characteristic impedance of the line and cause mismatch losses.

Researchers have combined these two methods of spurious suppression to achieve superior out-of-band rejection performance. In [12], a SIW bandpass filter uses multiple shapes for the resonators that have different higher-order modes and defects in the ground plane to suppress the spurious higher-order responses of the filter. These two methods combined successfully suppress the spurious responses of the filter, but the filter has a greater loss due to radiation and reflections, and increased design complexity. Compared to previous methods, this thesis proposes spurious suppression techniques that keep the inherent structure of the component and cause no radiation issues for integrated and embedded components (See Table 1.1).

Suppression Technique	No Radiation	No Reflections	Simple Geometry	Integrated	Embedded
Coupled-Line BPF with Capacitive Termination [11]	✓	✓	x	✓	x
Coupled-Line BPF with DGS [13]	x	x	✓	x	x
SIW BPF with Multi-Shape Resonators and DGS [12]	x	x	x	x	x
Proposed Techniques	✓	x	✓	✓	✓

Table 1.1: Comparison of Spurious Suppression Techniques.

1.3 SISL Technology

Suspended Integrated Stripline (SISL) is a recently developed transmission line technology that is fully board-embedded and capable of low losses. Unlike traditional planar transmission line technologies like microstrip and coplanar waveguide, the SISL transmission line is enclosed by conducting walls and vias, leading to little to no radiation losses [4]. Unlike conventional stripline that is surrounded by a dielectric material, SISL technology has its electromagnetic (EM) fields propagate mostly through air, reducing dielectric losses. Unlike suspended air stripline technologies that require extra mechanical housing [15, 16], SISL technology is fully board-embedded to make it easy to integrate into multi-layer printed circuit board (PCB) microwave systems [17].

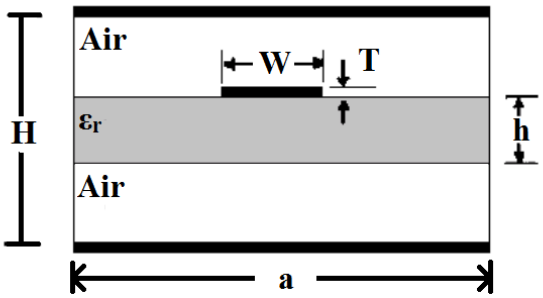

Figure 1.3: Cross section of Suspended Stripline [18]

Any SISL component consists of at least five layers. The top and bottom layers are sacrificial ground planes that enclose the air cavity and the suspended substrate. The top and bottom middle layers are cut out to create an air cavity for the suspended line. The center layer is a thin substrate with a low dielectric constant and loss that suspends the stripline. A cross section of the SISL stackup is shown in Fig. 1.3 and an isometric exploded view of a SISL Thru-line along with its metal layers is shown in Fig. 1.4.

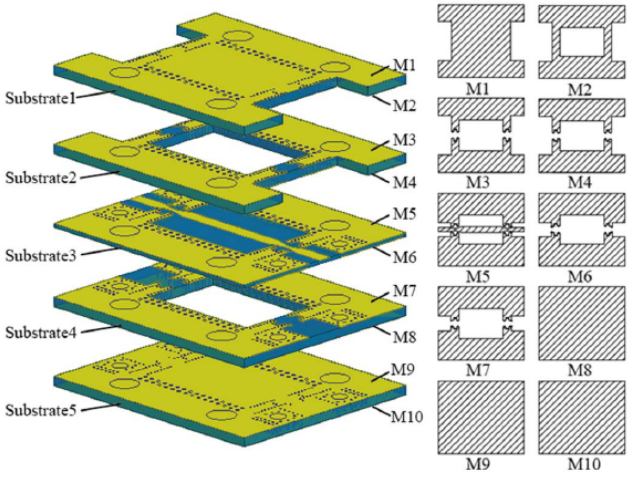

Figure 1.4: PCB Stack-up of SISL Thru-line [19]

1.4 Research Objectives

In this thesis, two new methods for suppressing spurious responses in SISL technology are proposed. The proposed designs use aperture coupled SIW resonators and resonant ground structures to eliminate the spurious responses of a distributed filter. These methods enhance the out-of-band performance of integrated and embedded microwave components.

1.5 Thesis Outline

Chapter 2 demonstrates the design of a SISL low-pass filter (LPF). The chapter walks through the step-by-step process used to create a 5th order Generalized Chebyshev filter with a 3 GHz cutoff frequency. The design is validated in both simulations and measurements. The chapter concludes by showing the modal analysis of the filter's spurious responses.

Chapter 3 explores aperture coupled SIW resonators for spurious response suppression. The theory of cavity resonators is discussed, and SIW is introduced as another board-integrated technology that can be combined with SISL. Design parameters are explored, and design steps are presented for aperture coupled SIW resonators. The designed aperture coupled SIW resonators are then simulated in the filter designed in the previous chapter to suppress spurious responses.

Chapter 4 explores resonant ground structures for spurious response suppression. The theory of resonant ground structures is explained in this chapter for spurious response suppression. Design parameters are explored, and design steps are presented for resonant ground structures. Integrated resonant ground structures are designed and simulated in the SISL filter to suppress spurious responses.

Chapter 5 details the fabrication of the embedded filter with resonant ground structures and shows the measured results. The measured results are analyzed to show improved performance and trade-offs in spurious suppression methods.

Chapter 6 concludes the thesis by providing a summary and suggestions for future work. This chapter suggests how to improve upon the discussed methods and offers new areas of exploration for spurious suppression in integrated and embedded microwave components.

Chapter 2

SISL Filter Design

A suspended integrated stripline (SISL) filter has been chosen to demonstrate the proposed spurious suppression techniques. Microwave filters are essential components in all microwave systems because they allow desired signals to pass through and attenuate any unwanted generated or received signals. Distributed microwave filters have many spurious responses that can allow unwanted signals to pass through the filter and destroy system performance. The SISL architecture was specifically chosen for its high-performance, low cost, and integrated and embedded design. SISL outperforms other architectures by having an enclosed suspended air cavity that reduces radiation and dielectric losses and makes it suitable for wideband applications [18]. SISL uses PCB substrates that are affordable and easy to fabricate, allowing for rapid prototyping. SISL is also an integrated and embedded component that poses unique challenges for spurious suppression. This chapter demonstrates a step-by-step process to design a 5th order Generalized low-pass Chebyshev filter with a cutoff frequency of 3 GHz and characterizes the spurious responses of the filter. The design of the SISL filter relies on the work done by Dr. Jay McDaniel and Dr. Kaixue Ma [18–25]. This filter acts as an architecture to test the spurious suppression techniques discussed in the following chapters.

2.1 Lumped Filter

The type of filter used in this work is a 5th order Generalized Chebyshev filter with a return loss of more than 20 dB in the passband and an insertion loss of more than 40 dB in the stopband.[1] A lumped-element filter is created using filter prototypes and transformations, and its response is simulated over frequency to verify the design.

2.1.1 Filter Prototypes and Transformation

The filter in this work is designed by using low-pass filter prototypes shown in Fig. 2.1 and Table 2.1 [26]. A Generalized Chebyshev filter was chosen for its high selectivity and linear phase. Selectively means that the filter has a sharp transition band that allows no signals just outside the operating frequency to pass through the filter. Linear phase in the passband decreases the chance of dispersion to occur in the system so all signals will have the same phase velocity.

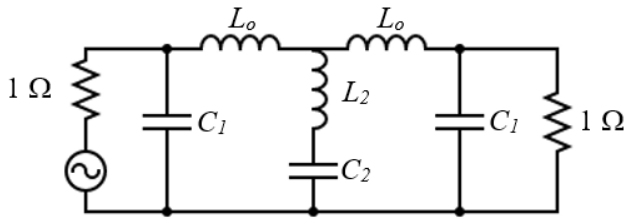

Figure 2.1: Schematic of Filter Prototypes

C_1	L_0	L_2	C_2
0.985092 F	1.2068 H	0.227543 H	1.37499 F

Table 2.1: Filter prototype values for Generalized Chebyshev

[1] It is important to note that both return loss and insertion loss are positive to describe the losses of the filter, even though they are often seen in S-Parameters as negative.

These low-pass filter prototypes are then transformed to have a characteristic impedance of 50 ohms and a cutoff frequency of $f_c = 3$ GHz using Equations 2.1 and 2.2

$$C = \frac{C_n}{R_o \omega_c} \tag{2.1}$$

$$L = \frac{R_o L_n}{\omega_c} \tag{2.2}$$

where $R_o = 50\,\Omega$, $\omega_c = 2\pi f_c$, $f_c = 3$ GHz, and C_n and L_n are the capacitor and inductor values of the filter prototype, respectively.

2.1.2 Simulated Results

The transformed values of the inductors and capacitors are then simulated in Microwave Office (MWO) using the schematic shown below, and the transformed values are found in Fig. 2.2 and Table 2.2. This filter produces a response that meets specifications of return loss and linear phase in the passband and insertion loss in the stopband as shown in Fig. 2.3 and Fig. 2.4.

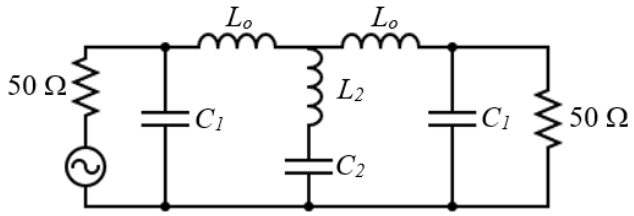

Figure 2.2: Schematic of Lumped-Element Generalized Chebyshev Filter

C_1	L_0	L_2	C_2
1.045 μF	3.201 nH	603.6 pH	1.459 μF

Table 2.2: Transformed values for Generalized Chebyshev

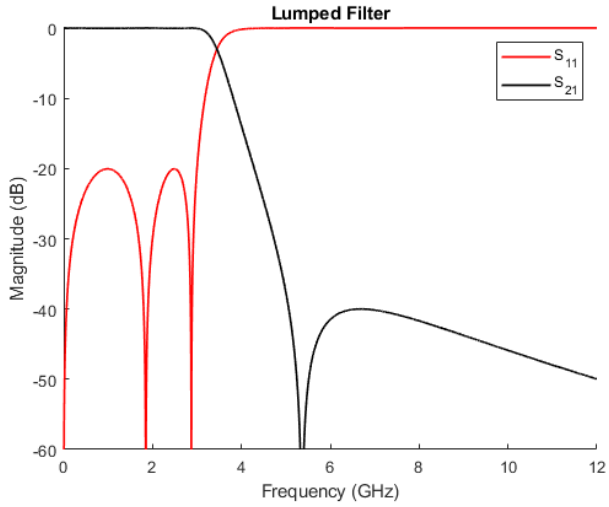

Figure 2.3: S-Parameters of Lumped-Element Generalized Chebyshev Filter

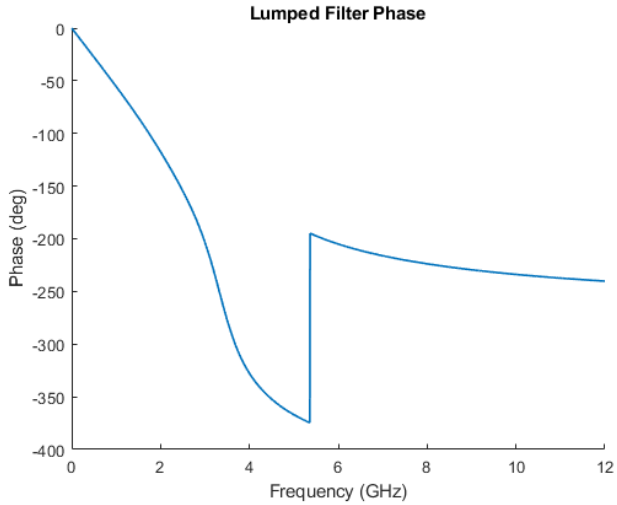

Figure 2.4: S_{21} Phase of Lumped-Element Generalized Chebyshev Filter

The lumped filter model is a stepping stone in the design of any filter and uses ideal lumped components. SISL technology uses commensurate stripline as effective inductors and capacitors to decrease the size of the filter [4]. The next step in the design of the SISL low-pass filter is to transform the ideal lumped components into commensurate stripline.

2.2 Effective Permittivity of SISL Cavity

The stripline in SISL technology sits on a very thin suspended dielectric substrate between two air cavities. The effective permittivity of the multi-layer substrate is close to that of air since most fields propagate through air. Some of the fields propagate through the thin dielectric substrate, which has a higher permittivity than that of air. To accurately design the SISL filter, the effective permittivity of the SISL structure needs to be determined. This is a crucial design step because an inaccurate effective permittivity will change the response of the filter drastically. A different effective permittivity will change the velocity of propagation to where the open stub filter will reflect electromagnetic waves differently, affecting the filter's expected performance. The effective permittivity of the SISL cavity was determined using Eigenmode simulation in HFSS. The cavity of the SISL structure was modeled with PEC side walls and a 10-mil Rogers 6002 substrate with a relative permittivity of 2.94 and a loss tangent of 0.0012. There are perfect H boundaries placed at each port to simulate the transition into the air cavity (see Fig. 2.5).

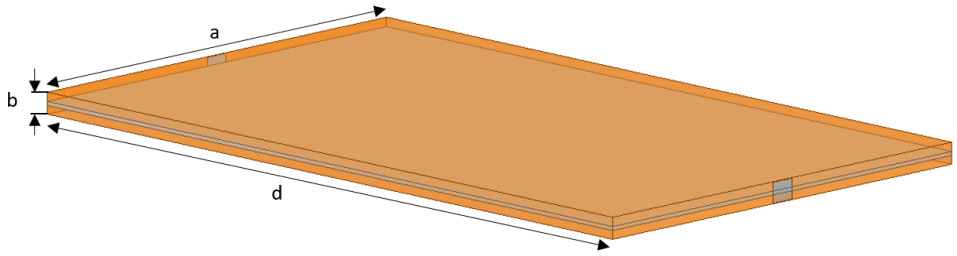

Figure 2.5: HFSS Model for Eigenmode Simulation

The simulated resonances of this structure with the estimated dimensions of the cavity (a = 30 mm, b = 50 mil, d = 50 mm) can determine the effective dielectric of

the cavity. The resonant frequency of a rectangular cavity is shown in Equation 2.3

$$f_{mnl} = \frac{c}{2\pi\sqrt{\mu_r \epsilon_{eff}}}\sqrt{\left(\frac{m\pi}{a}\right)^2 + \left(\frac{n\pi}{b}\right)^2 + \left(\frac{l\pi}{d}\right)^2} \tag{2.3}$$

where f is the resonant frequency, c is the speed of light, μ_r is the relative permeability, ϵ_{eff} is the effective permittivity, a, b, and d are the dimensions of the cavity, and m, n, and l are the mode numbers of the resonant frequency. This equation is rearranged to solve for the effective permittivity.

$$\epsilon_{eff} = \frac{c^2}{4\pi^2 f^2 \mu_r}\left(\left(\frac{m\pi}{a}\right)^2 + \left(\frac{n\pi}{b}\right)^2 + \left(\frac{l\pi}{d}\right)^2\right) \tag{2.4}$$

The HFSS Eigenmode simulation gave a resonant frequency of 5.469 GHz for the dominant mode (f_{101}). Using Equation 2.4, this yields an effective permittivity of approximately ϵ_r = 1.147 for the SISL cavity.

2.3 Distributed Filter

Having determined the effective permittivity of the SISL cavity, it is possible to accurately model the filter as stripline in MWO. The open stub stripline filter will have spurious responses that appear due to the harmonics and periodicity of the commensurate line.

2.3.1 Distributed Transformations

The stripline structure is created using Richard's transformation and Kuroda's identities. Richards transformation changes the ideal lumped components into transmission line sections, and Kuroda's identities use redundant transmission line sec-

tions to achieve more practical microwave filter implementations by converting between open and short stubs [4]. Both Richard's transformation and Kuroda's identities are used to derive design equations in [18] for the length and widths of stripline for the shunt LC circuits and series inductors. Below are the design equations used in this work for the length and width of the shunt LC circuits.

$$l_{shunt\,inner\,stub} = \frac{c}{\pi f_c \sqrt{\epsilon_{eff}}} \tan^{-1}\left(\frac{1}{\omega_o}\right) \tag{2.5}$$

$$l_{shunt\,outer\,stub} = \frac{l_{shunt\,inner\,stub}}{2} \tag{2.6}$$

$$w_{shunt} = \frac{b-t}{4}\left(\frac{1.2\omega_o C_2}{\sqrt{\epsilon_{eff}}} - 4 \cdot \frac{C_f}{\epsilon}\right) \tag{2.7}$$

where c is the speed of light, f_c is the cutoff frequency, b is the total height of the SISL cavity, t is the thickness of the stripline, and ϵ_{eff} is the effective permittivity of the SISL cavity. ω_o is a variable that ensures that the transmission zeros occur near the band edge and for this filter prototype it is 1.7878. $\frac{C_f}{\epsilon}$ accounts for the fringing capacitance of the stripline structure and can be approximated for an infinitely thin conductor as 0.4413.

Below are the design equations for the length and width of series inductors [18]

$$l_L = \frac{Z_{term} L_o}{30\pi} \cdot \left[\frac{2.375 \cdot b \cdot e^{\frac{-5\sqrt{\epsilon_{eff}}}{6}}}{b-t} + \frac{C_f}{\epsilon}\right] \frac{c}{2\pi f_c} \tag{2.8}$$

$$w_L = \frac{1.9 \cdot b}{0.8 e^{\frac{5\sqrt{\epsilon_{eff}}}{6}}} \tag{2.9}$$

where Z_{term} is 50 ohms for a 50-ohm system. Using these design equations and the optimizer in MWO, a suspended stripline filter was designed. The layout of the filter and a table with the dimensions are shown in Fig 2.6 and Table 2.3, respectively.

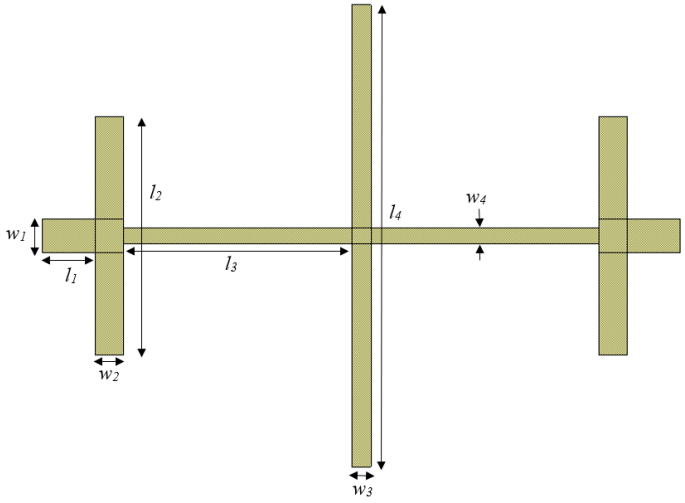

Figure 2.6: MWO Layout of Distributed Generalized Chebyshev Filter

Variable	**Length (mm)**	**Variable**	**Length (mm)**
l_1	2.984	w_1	1.848
l_2	13.448	w_2	1.622
l_3	12.84	w_3	1.087
l_4	26.027	w_4	0.9067

Table 2.3: Dimensions of MWO Distributed Filter

2.3.2 Simulated Results

The filter with the dimensions shown above is simulated in MWO, and the frequency response is shown in Fig. 2.7. Compared to the lumped filter response presented earlier, the distributed filter has a spurious response located close to 8.5 GHz. Spurious responses like these are common in open stub distributed filters and are periodic in frequency.

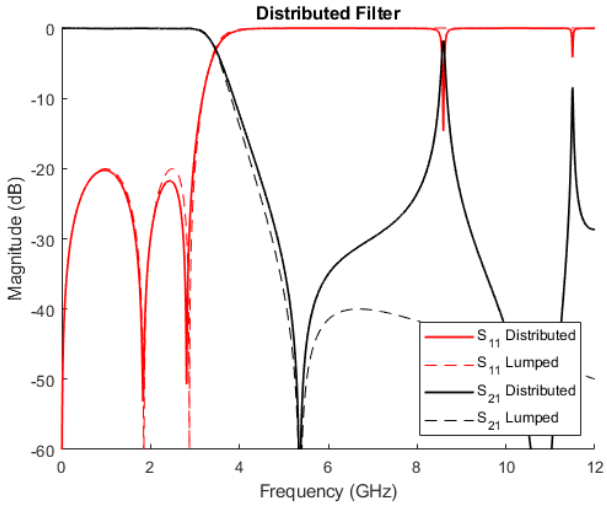

Figure 2.7: S-Parameters of Lumped and Distributed Generalized Chebyshev Filters

The filter was simulated over a larger frequency to show that the response is periodic in frequency with a period of roughly 22 GHz. This periodic nature is due to Richard's transformation ($\Omega = \tan \beta l$) that repeats every time βl is a multiple of π because of the tangent function in the equation. The modal analysis in Section 2.5 explains in greater detail the nature of the spurious response in the distributed filter.

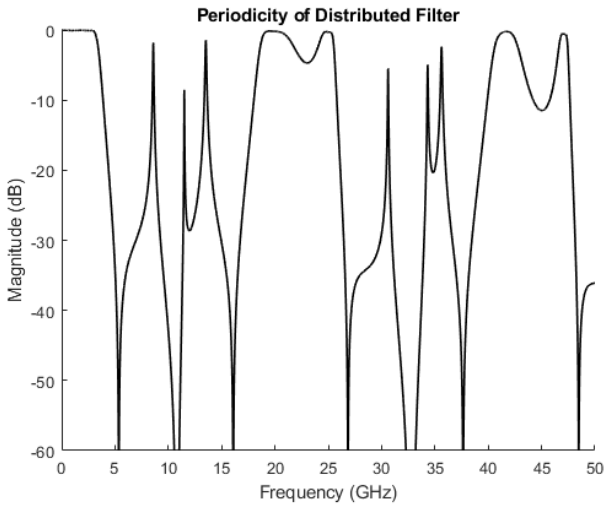

Figure 2.8: Periodic S_{21} of Distributed Generalized Chebyshev Filter

2.4 HFSS Filter Model

The dimensions used in the MWO filter were modeled and simulated in HFSS to create a more robust model by using a finite element method solver that accounts for resonances and other spurious effects. This filter meets the design specifications and has the same stackup as the thru-line shown in Chapter 1 (See Fig. 1.4). Substrate 1 and Substrate 5 for the sacrificial top and bottom layers are both 30-mil thick Rogers 4350B substrates. Substrates 2 and 4 that create the air cavity are both 20-mil thick Rogers 6002 substrates.

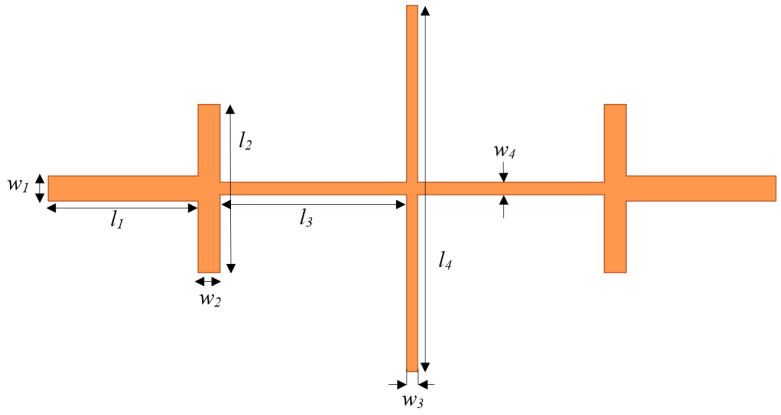

Figure 2.9: HFSS Layout of Distributed Generalized Chebyshev Filter

Variable	**Length (mm)**	**Variable**	**Length (mm)**
l_1	10	w_1	1.75
l_2	11.5	w_2	1.5
l_3	12.8364	w_3	0.75
l_4	25.1163	w_4	0.85

Table 2.4: Dimensions of HFSS Distributed Filter

2.4.1 SISL Cavity Model

The first step in simulating any SISL structure is to simulate the suspended stripline in an ideal cavity. The cavity in the HFSS is surrounded by PEC walls to enclose the fields instead of a via cage. The cavity model simulates a suspended line on a 10-mil Rogers 6002 substrate with a dielectric constant of 2.94 and a loss tangent of 0.0012. The air cavity is enclosed on top and bottom by two sacrificial substrate layers that provide the return currents for the suspended stripline. The exploded HFSS model of the SISL air cavity is shown in Fig. 2.10, and the results are shown in Fig 2.11. The responses of MWO and HFSS models differ in the stopband due that the filter dimensions changing and to the spurious standing-wave effects discussed in Section 2.5 being more accurately modeled in HFSS.

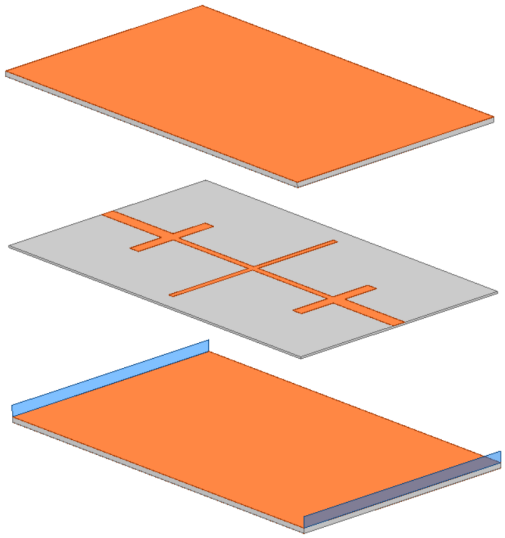

Figure 2.10: Exploded View of SISL Cavity Model

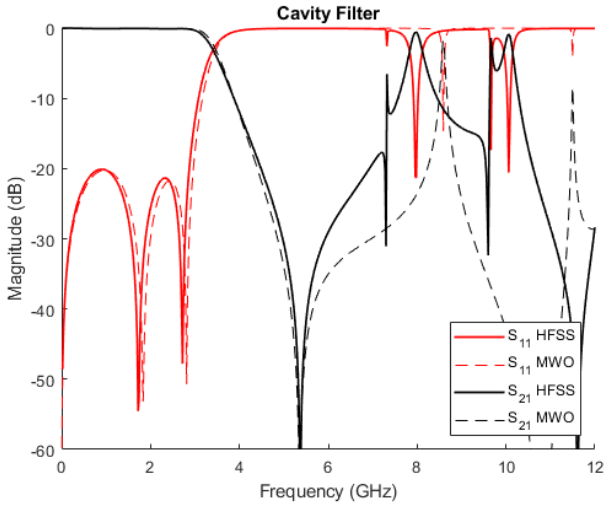

Figure 2.11: S-Parameters of MWO and HFSS Cavity Filters

The SISL cavity itself can act as a cavity resonator or a waveguide to create spurious responses. The sharp spikes in S_{21} and dips in S_{11} are the resonances of SISL cavity where the dimensions of the cavity create a 2D standing wave. Fig. 2.12 shows the electric fields of the cavity resonance at 9.66 GHz where there is a 2D standing wave of 1 $\frac{1}{2}$ wavelengths (λ).

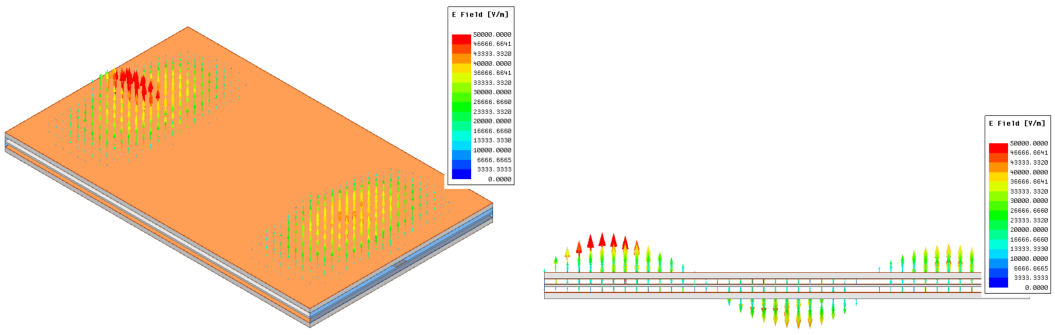

(a) Isometric View (b) Side View

Figure 2.12: Electric Fields of Cavity Resonance at 9.66 GHz

2.4.2 Shrinking the SISL Cavity

The resonances of the air cavity can destroy the performance of the stopband. These resonances can be "pushed out" by reducing the size of the air cavity, which will increase the resonant frequency (see Equation 2.3). There is unused space in the air cavity next to the outer stub of the filter. This space can be cut out of the air cavity to increase the resonant frequency of the air cavity structure while still maintaining a stable effective permittivity. The exploded isometric view of HFSS is shown in Fig. 2.13, and the response of the filter is shown in Fig 2.14. The resonances of the air cavity are "pushed out" in frequency. The first resonance of the cavity moved up in frequency from 6.54 GHz to 9.14 GHz due to shrinking the dimensions of the cavity.

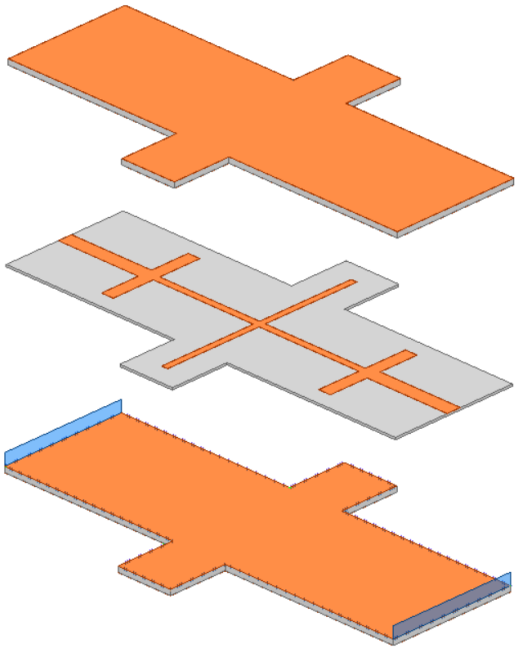

Figure 2.13: Exploded View of Shrunk SISL Cavity Model

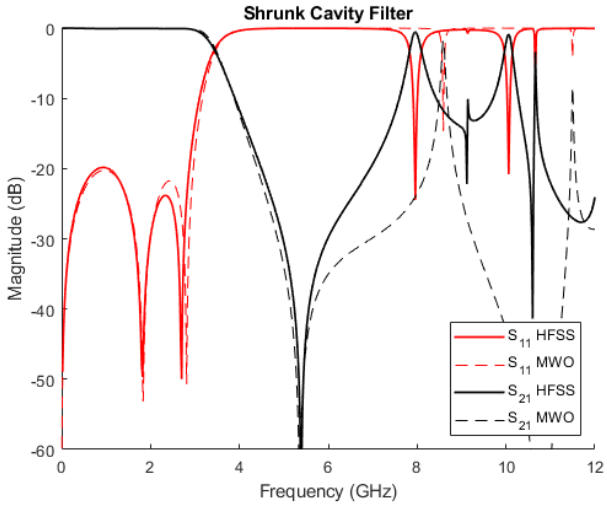

Figure 2.14: S-Parameters of MWO and HFSS Filters for Shrunk Cavity

2.4.3 CPWG-SISL Transition

For the SISL filter to be measured, the air cavity model needs to transition to a structure that can connect to edge launch connectors. In [19], a novel transition from Grounded Coplanar Waveguide (CPWG) to SISL is proposed and verified. The transition used in this work connects the SISL filter structure to edge launch connectors for measurements and is shown in Fig 2.15. The transition works by tapering into a small substrate suspended stripline and tapering out to the SISL air cavity to maintain a 50-ohm match between the different transmission line structures. This transition structure is tuned in HFSS by attaching the transition to a SISL thru-line and varying the distance between the signal trace to the side ground plane of the CPWG to maintain a 50-ohm characteristic impedance up to the 3 GHz cutoff frequency.

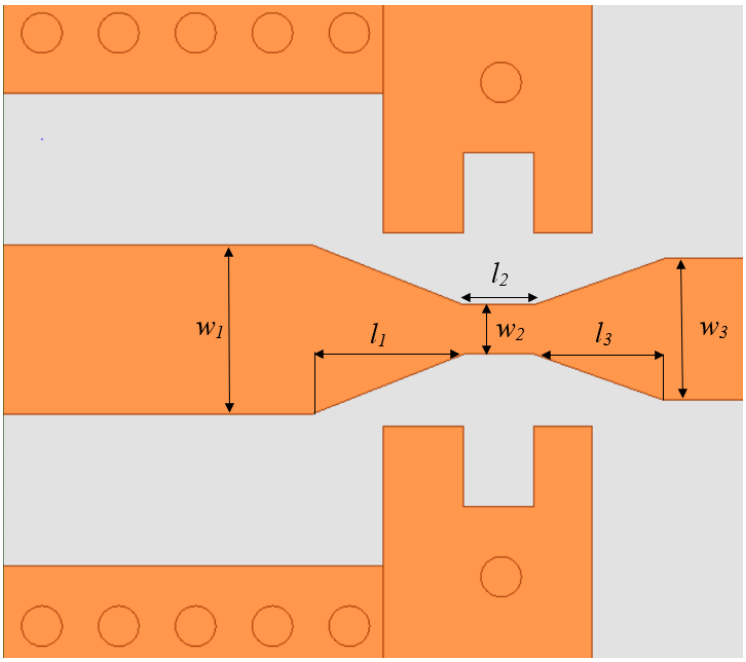

Figure 2.15: CPWG-SISL Transition

Variable	**Length (mm)**	**Variable**	**Length (mm)**
l_1	1.889	w_1	2.1
l_2	0.867	w_2	0.61
l_3	1.607	w_3	1.75

Table 2.5: Dimensions of CPWG-SISL Transition

CPWG is a very common transmission line in printed circuit boards because it contains fields better than a microstrip line. It consists of a center signal trace, two coplanar ground planes on either side of the signal trace, and a lower ground plane below the signal trace. This is the transmission line that will transition into and out of the stripline cavity to connect to edge launch connectors. CPWG is a well-defined transmission line that can be tuned to a characteristic impedance of 50 Ω by adjusting the width of the trace and the distance between the side grounds [27].

2.4.4 Full Filter Model

With the transition tuned, the last stage of the SISL filter design is to attach the transitions to the cavity model to simulate the entire filter model. An exploded isometric view of the full SISL stackup is shown in Fig. 2.16. Instead of having PEC walls like the cavity filter model, the SISL air cavity is surrounded by a cage of vias to contain the EM fields. The via cage is present on all the layers of the SISL filter to suppress any parallel plate modes that could be excited by the transition.

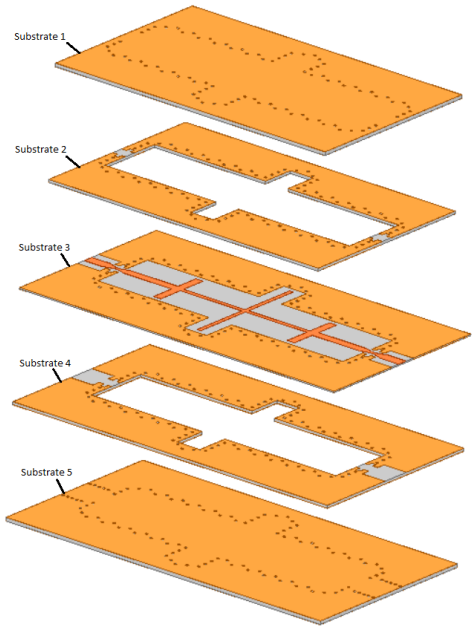

Figure 2.16: Exploded View of SISL Stackup

2.4.5 Simulated Results

The HFSS simulated results of the SISL filter are shown in the figure below. The simulated results of the full embedded SISL filter meet the filter specifications of more than 20 dB of return loss in the passband and have similar spurious responses at 8 and 10 GHz.

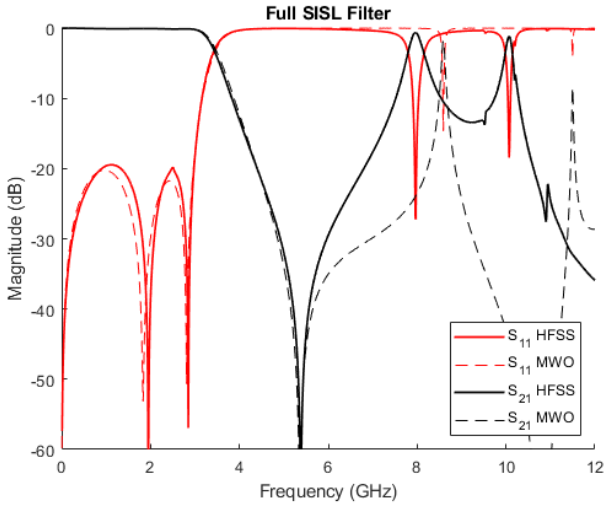

Figure 2.17: S-Parameters of MWO and HFSS Filters

2.4.6 Measured Results

The filter was fabricated using the LPKF U4 Protolaser and measured on the Agilent Technologies N5225A PNA that was calibrated using an Agilent N4691-60006 electronic calibration module. The measured results have a different shape to S_{11} in the passband, and this is most likely due to the edge launch connectors that were not included in the simulated design. The same spurious responses appear in the measured results as the simulated results. The following chapters explore techniques to suppress the spurious responses at 8 and 10 GHz. More detailed discussions on fabrication and measurements are found in Chapter 5 and Appendix A.

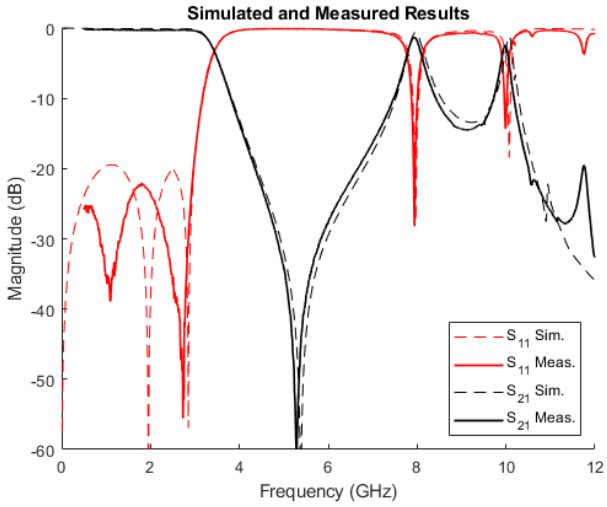

Figure 2.18: S-Parameters of Simulated and Measured Filters

2.5 Modal Analysis of Spurious Responses

The final SISL simulation has two noticeable spurious responses. A lumped filter will attenuate all the signals at frequencies outside the stopband but because of the distributed filter's geometry, there will be standing waves that cause spurious transmission. The filter is simulated in HFSS at 8 and 10 GHz to understand the standing wave phenomenon that causes spurious transmission for this particular microwave component. At these frequencies, there are significant standing waves created on the distributed filter that allow for spurious transmission. The signals at these frequencies are not reflected back and travel as standing waves on the open stub filter due to its inherent geometry.

Kuroda's identity that converts short stubs to open stubs for ease of fabrication and design uses extra transmission lines to transform and connect the stubs. These extra pieces of transmission are the elements of the filter that resonate at these frequencies and allow for standing waves to propagate through the filter. These standing waves that allow for spurious transmission need to be reflected back, which is

done using the spurious suppression techniques discussed in the following chapters. Below are figures showing the vectors of the electric field that propagate as standing waves across the filter at 8 and 10 GHz.

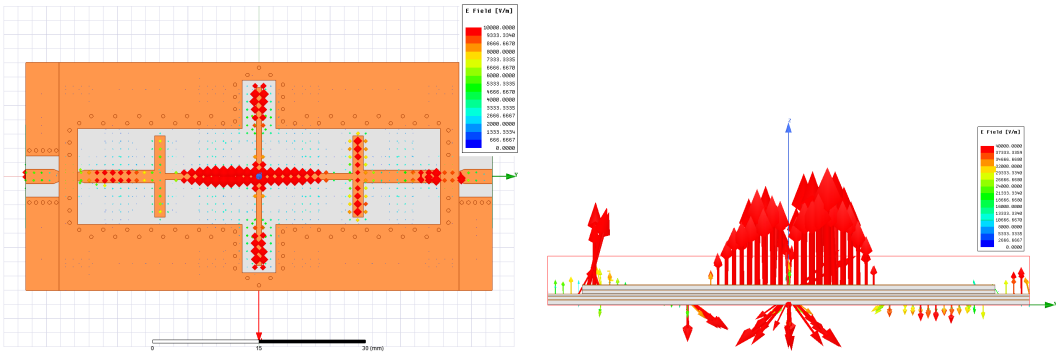

(a) Top View (b) Side View

Figure 2.19: Modal Analysis at 8 GHz

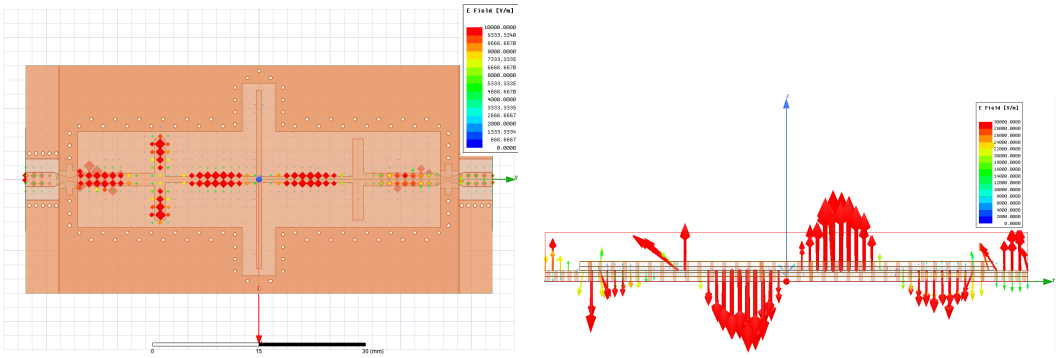

(a) Top View (b) Side View

Figure 2.20: Modal Analysis at 10 GHz

For this work, the spurious responses of the filter at 8 and 10 GHz are suppressed using different techniques. The goal of the spurious suppression is to lower the transmission of the filter below -10 dB at and around 8 and 10 GHz. Chapters 3 and 4 explore two different techniques to suppress the spurious responses to the goal level of -10 dB in S_{21}.

Chapter 3

Aperture Coupled SIW Resonators

Substrate Integrated Waveguide (SIW) is another planar embedded technology used in integrated RF and microwave systems [28]. SIW structures act like dielectric-filled waveguides and have via fences for sidewalls as shown in Fig 3.1. SIW resonators are cost-effective, high-Q building blocks for selective RF filters [29]. SIW resonators are relatively easy to design and are well understood based on fundamental cavity resonator theory [4].

This chapter explores the method of using aperture coupled SIW resonators to suppress the spurious responses of the filter. The sacrificial top and bottom ground layers are essentially substrate-filled cavities that can be coupled into to reflect or absorb spurious responses. Traditionally, designers couple into SIW using transmission lines such as microstrip or CPWG, but recent techniques have explored using apertures to couple into SIW. Aperture coupled SIW has been used to excite an array of patch antennas [30] and transition from an inner layer to microstrip [31], but aperture coupled SIW has not been used in SISL to the author's knowledge. SIW resonators are an intuitive method for suppressing spurious responses in SISL.

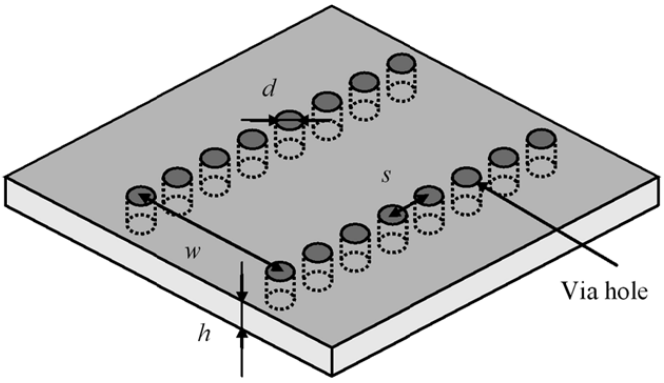

Figure 3.1: Substrate Integrated Waveguide [32]

3.1 Cavity Resonator Theory

Cavity resonators are sections of a waveguide that have two shorted ends to form a cavity. According to the dimensions of the structure, an electromagnetic wave will resonate at a frequency for any given mode. Cavity resonators are building blocks for many bandpass filters with high quality factor and selectivity. The quality factor of a resonator is inversely proportional to the bandwidth of the resonator ($Q \propto \frac{1}{BW}$). The resonant frequency for a given mode for a rectangular cavity is shown in Eq. 2.3 that was used in the previous chapter to calculate the effective permittivity of the SISL cavity. For an SIW resonator, the resonant frequency will be slightly lower than a dielectric-filled waveguide with the same dimensions because some of the fields will bend around the gaps in the vias. This bending increases the effective size of the cavity and reduces the resonant frequency as shown in Fig. 3.2

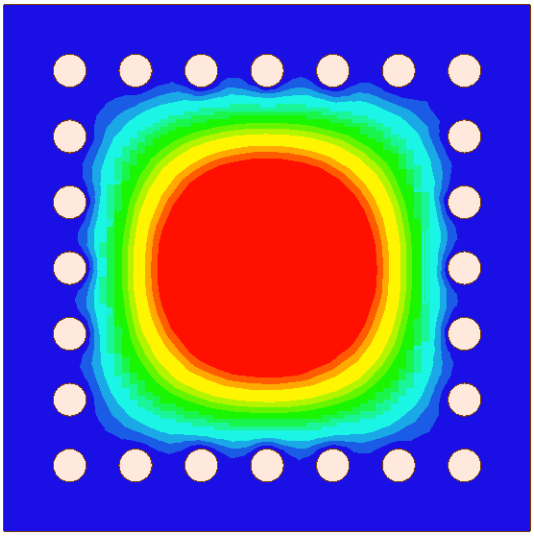

Figure 3.2: Magnitude of Electric Field in SIW

3.2 Aperture Coupling Theory

There are two kinds of aperture coupling: electric and magnetic coupling. Electric coupling is when energy is transferred from one structure to another through the electric field. Similarly, magnetic coupling is when energy is transferred from one structure to another through the magnetic field. Any aperture coupling will have a combination of electric and magnetic coupling. To primarily electrically couple into an SIW resonator, the aperture must be at the center of the resonator where the electric field is at a maximum value. Conversely, to primarily magnetically couple into an SIW resonator, the aperture must be on the edge of the resonator where the magnetic field is at a maximum value. For coupling from a suspended line to SIW, magnetic coupling transfers the most energy and maximizes suppression. The aperture is located directly above the suspended stripline where the maximum electric and magnetic fields will occur.

3.3 Design Parameters

An aperture coupled SIW resonator is simulated in HFSS using a SISL cavity model with a suspended thru-line as shown in Fig. 3.3. The EM fields from the suspended line couple into the SIW cavity resonator, which resonates and reflects the waves at its resonant frequency. In this work, two design parameters that affect the suppression performance of the SIW resonator are studied and explored.

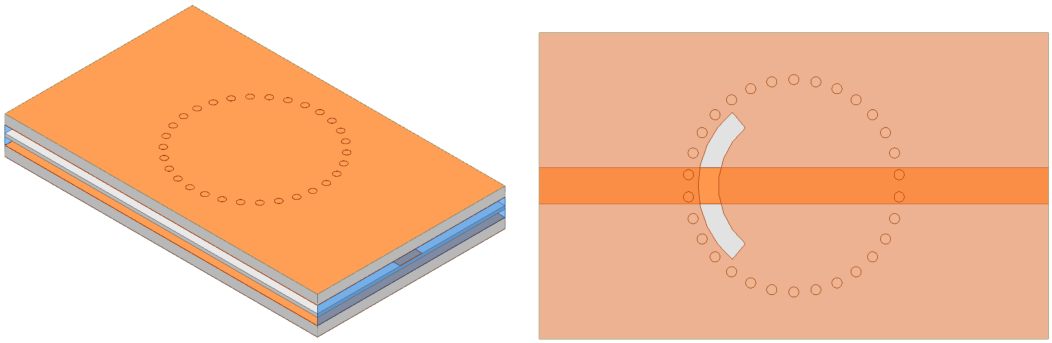

(a) Isometric View (b) Top View

Figure 3.3: SIW Cavity Model

The first parameter studied in this work is the geometry of the resonator. The two most common geometries for SIW resonators explored here are rectangular and circular resonators. Both rectangular and circular cavities were designed to resonate at 10 GHz and have approximately the same aperture size of 15 mm^2. The S-parameters for square and circular SIW resonators are compared in Fig. 3.4. The circular SIW resonator has much greater suppression than the square SIW resonator for the same resonant frequency and size of the aperture. Circular SIW resonators outperform square resonators because the magnetic fields that couple into the SIW naturally flow in a circle at the fundamental resonant mode. Therefore, the circular resonator provides a better structure for the magnetic fields to resonate. The resonant frequency of the dominant TM_{010} mode for an aperture coupled SIW resonator

can be found using Equation 3.1 [4]

$$f_{mnl} = \frac{c}{2\pi\sqrt{\mu_r \epsilon_r}} \sqrt{\left(\frac{p_{nm}}{a}\right)^2 + \left(\frac{l\pi}{d}\right)^2} \tag{3.1}$$

where f_{mnl} is the resonant frequency, c is the speed of light, μ_r is the relative permeability, ϵ_r is the relative permittivity, a is the radius of the resonator, d is the height of the resonator, and p_{mn} and l are parameters dependent on the mode. For the dominant TM_{010} mode, $p_{01} = 2.405$ and $l = 0$. The superior suppression of the circular aperture coupled SIW resonator shown clearly in Fig. 3.4.

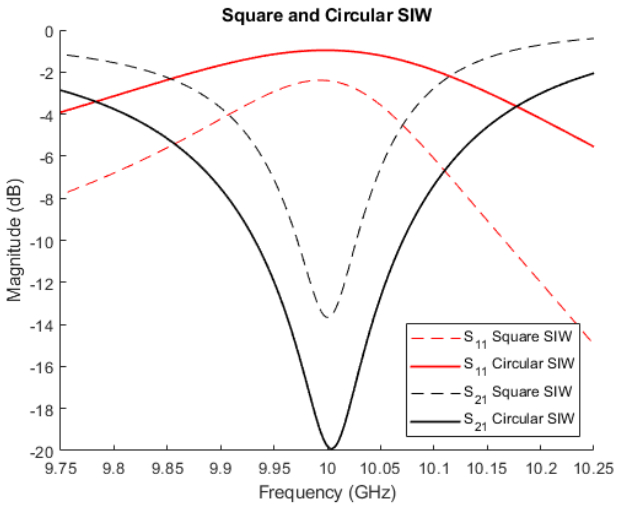

Figure 3.4: Square and Circular SIW

The second parameter studied in this work is the size of the aperture. The size of the aperture directly affects the coupling between the suspended line and the SIW resonator. The size and shape of the aperture also change the resonant frequency of the SIW resonator. Two different dimensions of the aperture were varied in a parametric sweep to find the maximum suppression of the SIW resonator.

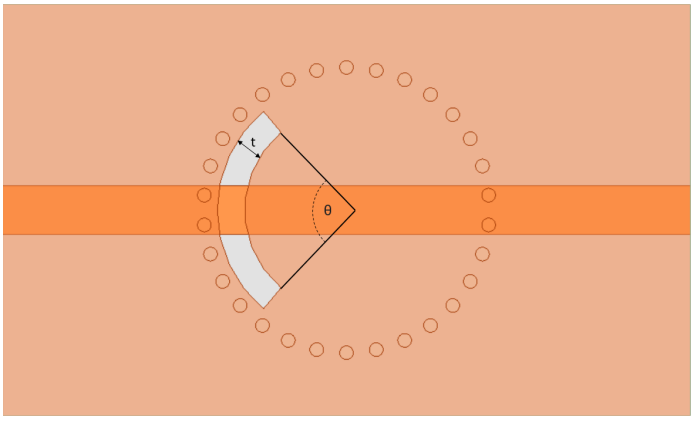

Figure 3.5: Dimensions of aperture: angle θ and thickness t

The first aperture dimension varied is the arc angle (θ) of the aperture (see Fig. 3.5). The arc angle was varied from 90° to 150° to find the maximum suppression of the SIW resonator and the simulated results are shown in Fig. 3.6. The transmission drop-out in S_{21} is shown for different arc angles of the aperture. The deepest suppression is 22 dB at an arc angle of 150°. The resonant frequency decreases as the arc angle increases because the excited current in the resonator has a longer distance to travel and creates an inductive effect.

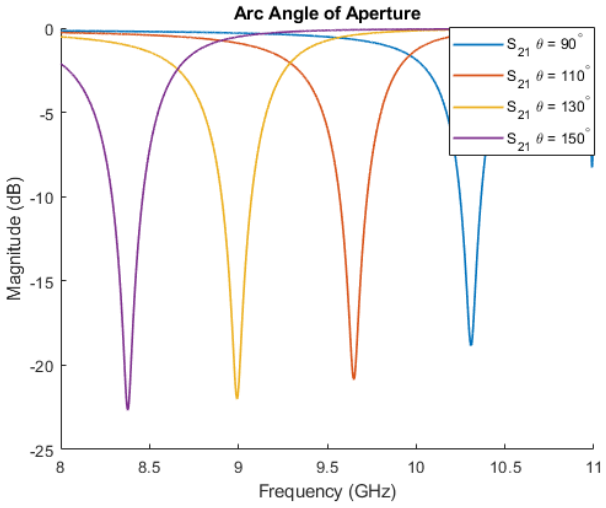

Figure 3.6: S_{21} of Varied Arc Angle (θ)

The next aperture dimension varied is the thickness t of the aperture (see Fig. 3.5). The thickness of the aperture was varied from 1 mm to 3 mm with the arc angle of the aperture fixed at 150°. The thickness did not significantly change the suppression level due to the SIW resonator as shown in Fig. 3.7. The resonant frequency increases as the arc thickness increases because the thickness of the aperture reduces the effective size of the resonator, thus shifting the resonance up in frequency.

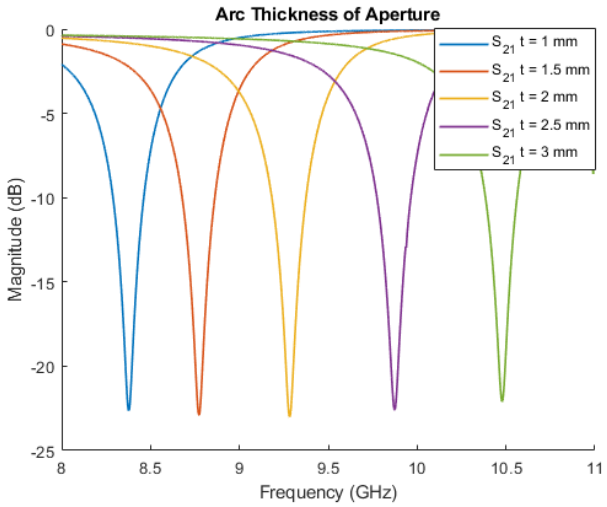

Figure 3.7: S_{21} for Varied Thickness (t)

3.4 Design Steps

Using the parameter study above, a design process is developed for creating aperture coupled SIW resonators for spurious suppression. A substrate must be chosen for the SIW resonator that keeps the dimensions of the cavity small. Higher permittivity substrates allow for smaller SIW resonators and save valuable board space. Next, the dimensions of the cavity resonator need to calculated using Equation 3.1 for the desired resonant frequency. The design is then simulated with the calculated dimensions of the SIW resonator to verify the desired resonant frequency. The di-

mensions of the SIW resonator are then altered to account for the effects of the aperture. A design flow graph of the process in shown in Fig. 3.8.

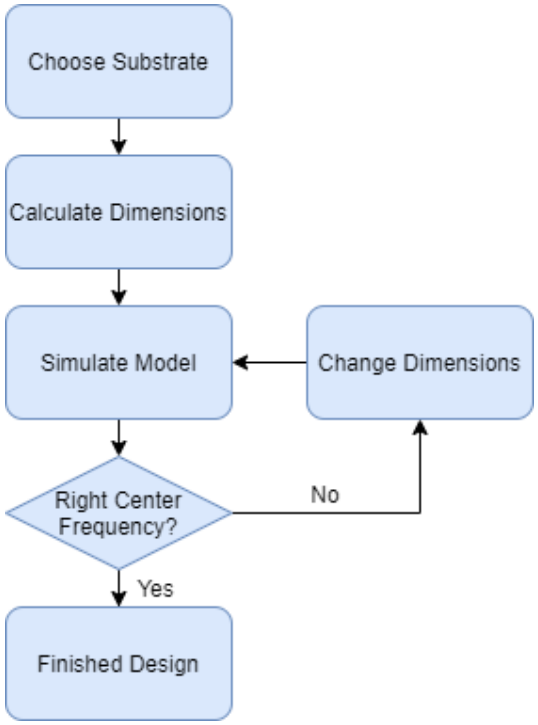

Figure 3.8: Aperture coupled SIW Resonator Design Flow Graph

3.5 Simulated Results

After the aperture coupled SIW resonators have been designed to the correct center frequency, they can be placed on the input of the filter to test the signal suppression. The aperture coupled SIW resonator is simulated for suppressing the spurious responses at 8 and 10 GHz and the cavity resonance at 9.14 GHz in the HFSS model shown in Fig. 3.9. The shrunk cavity model of the filter is used to simplify the design and save simulation time.

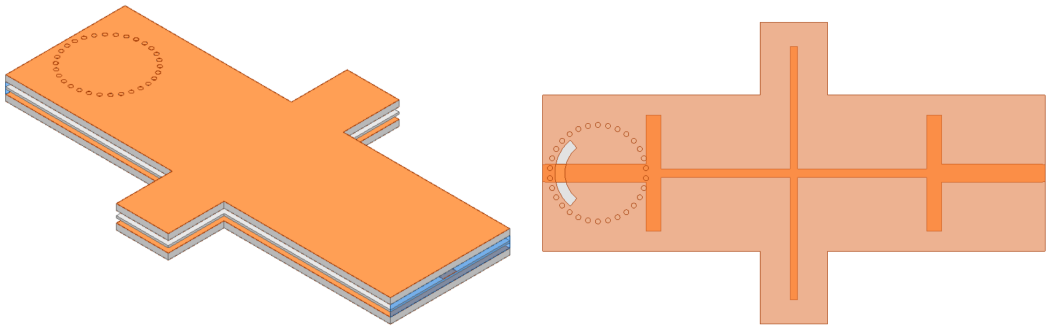

(a) Isometric View (b) Top View

Figure 3.9: Filter Cavity SIW Model

Adding the aperture coupled SIW resonators does not greatly affect the pass-band of the filter while providing suppression in the stopband. An aperture coupled SIW resonator was designed to resonate at 8 GHz to suppress the first spurious response of the filter. The aperture coupled SIW resonator designed at 8 GHz partially suppresses the first spurious response of the filter from -0.5 dB to -2 dB in S_{21} and increases S_{11} in the passband by 0.1 dB. Even though there is a noticeable notch in the transmission at 8 GHz, the suppression bandwidth is not large enough to suppress the first spurious response of the filter (see Fig. 3.10).

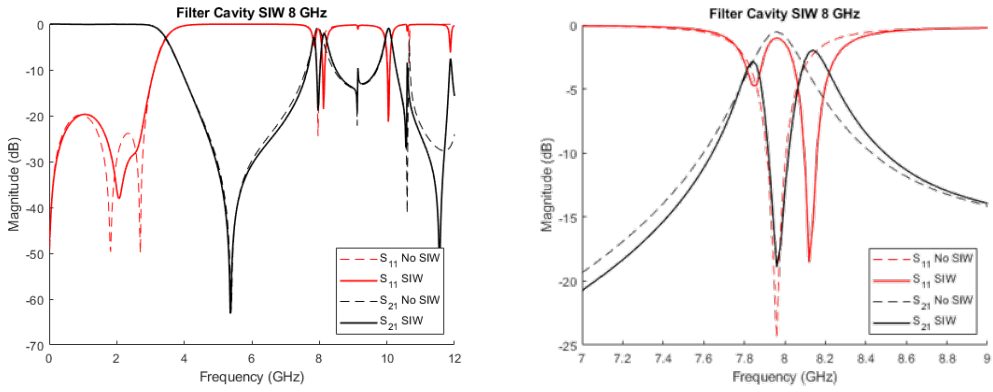

(a) Filter Response (b) Spurious Suppression

Figure 3.10: Cavity Filter with SIW at 8 GHz

Next, an aperture coupled SIW resonator was designed to resonate at 10 GHz to suppress the second spurious response of the filter. This aperture coupled SIW resonator again partially suppresses the second spurious response of the filter from -0.9 to -3.5 dB in S_{21} as shown in Fig. 3.11. Even though there is a noticeable notch in the transmission at 10 GHz, the suppression bandwidth is not large enough to suppress the second spurious response of the filter.

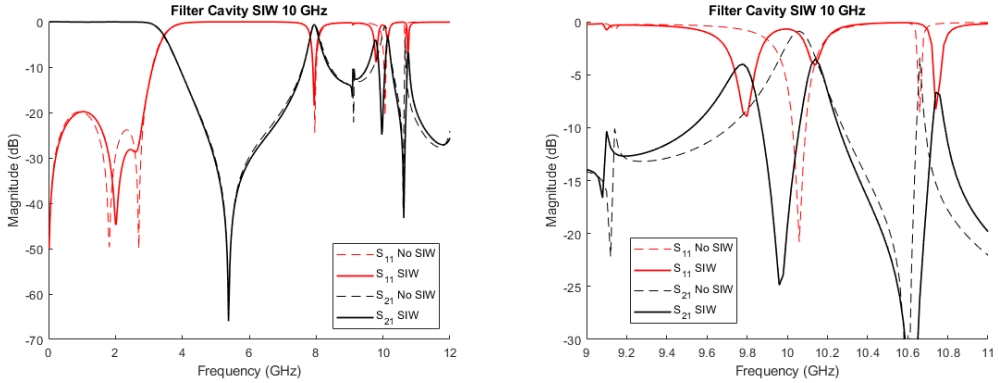

(a) Filter Response (b) Spurious Suppression

Figure 3.11: Cavity Filter with SIW at 8 GHz

Lastly, an aperture coupled SIW resonator was designed to resonate at 9.14 GHz to dampen the first spurious cavity resonance of the filter. This aperture coupled SIW resonator dampens the first spurious cavity resonance of the filter and pushes it out in frequency. This dampening occurs because the magnetic fields of the first cavity resonance couple into the SIW cavity resonator and reflect this resonance. The cavity still wants to resonate at the first resonance, so the cavity becomes effectively smaller for the magnetic field to avoid coupling into the aperture, increasing the resonant frequency.

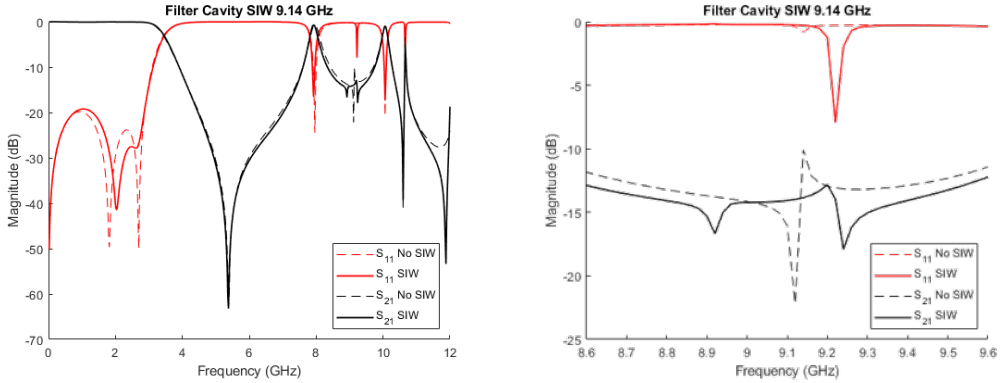

(a) Filter Response (b) Spurious Suppression

Figure 3.12: Cavity Filter with SIW at 8 GHz

3.6 Conclusions

For any given resonator, there is a fundamental coupling limitation that determines the maximum suppression from the SIW resonator. Even though SIW resonators have a straightforward and intuitive design, the fundamental coupling and bandwidth limitations make them less suitable for signal suppression and other techniques need to be explored. Aperture coupled SIW resonators have been shown in simulation to dampen the cavity resonances by dampening the fields in the dielectric. Aperture coupled SIW resonators do not provide sufficient suppression for the spurious responses of the design SISL LPF. The next chapter explores another spurious suppression technique to adequately suppress the spurious responses of the filter.

Chapter 4

Integrated Resonant Ground Structures

This chapter explores the theory of defected ground structures (DGS) and the method of using resonant ground structures (RGS) to suppress the filter's spurious responses. The integrated RGS is enclosed in a via cage instead of a metal cavity, making the technology useful for integrated microwave components. Resonant ground structures have a lower quality factor than aperture coupled SIW resonators that make them a better candidate for the wideband suppression needed to suppress the spurious responses of the filter. The design steps and parameters of resonant ground structures are explored in this chapter, resonant ground structures are designed to suppress the spurious responses and cavity resonances of the designed SISL filter.

4.1 Defected Ground Structure Theory

A recent trend in microwave component design is to intentionally modify the ground plane to increase performance. One intentional modification of the ground plane is called a defected ground structure (DGS), an etched-out portion of the ground plane. Unlike its name suggests, a defected ground structure is not defective but rather effective at enhancing the performance of microwave components such as

antennas [33], power dividers [34], branch-line couplers [35], and filters [36]. Defected ground structures redirect the return currents on the ground plane to create a resonant structure. At RF and microwave frequencies, the return currents are located directly under the signal trace. To disturb the return currents, defected ground structures are placed directly under the signal trace.

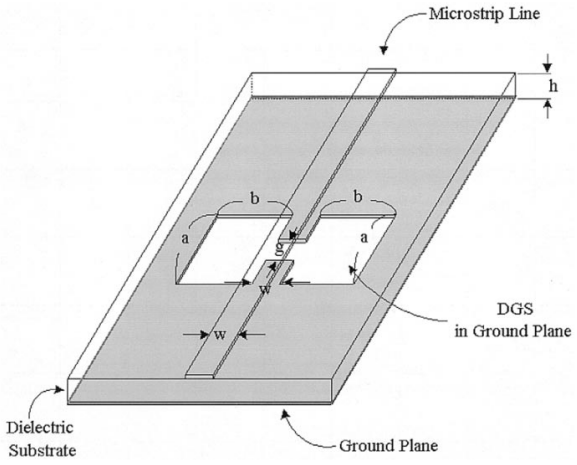

Figure 4.1: Barbell DGS in Microstrip Line [37]

A common DGS is a simple barbell DGS shown above in Fig. 4.1. Changing the physical dimensions of the square ends by varying their length and width (a and b) controls the inductance of the DGS. Return current must flow around the large sides of the defect, and this circulating current produces an inductance. Changing the physical dimensions of the center gap by varying its length and width (g and w) controls the capacitance of the DGS. The center gap looks electrically like a parallel plate capacitor and creates an edge capacitance where displacement currents can flow. The total DGS structure acts like a parallel LC circuit that resonates where the stored magnetic energy of the effective inductor equals the stored electric energy in the effective capacitor (see Fig. 4.2) [4]. Close to the resonant frequency of the DGS (see Equation 4.1), all the signals will be reflected back and will not pass

through the microstrip line. The bandwidth (BW) of the DGS is another important parameter and is inversely proportional to the quality factor (Q). The quality factor of the DGS depends on the effective inductance and capacitance of the DGS (see Equation 4.2).

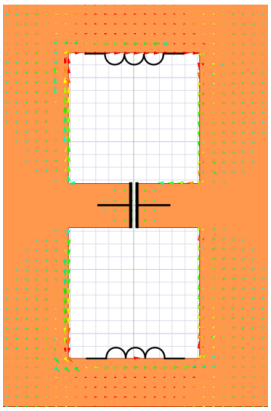

(a) Return Current Distribution of DGS with Circuit Symbols

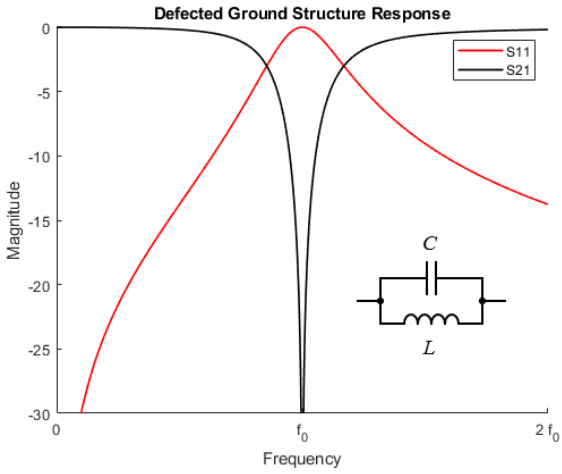

(b) Ideal Response of DGS

Figure 4.2: Ideal DGS Model

$$f_0 = \frac{1}{2\pi\sqrt{LC}} \tag{4.1}$$

$$Q_0 = \frac{R}{\omega_0 L} = \omega_0 RC \tag{4.2}$$

The main problem with DGS technology is that defects in the ground plane radiate like slot antennas, which are highly efficient radiators [14]. Radiation is difficult to model in enclosed microwave systems and can cause EMI and EMC issues if not shielded properly. Most often, microwave enclosures are flush against the chassis ground plane of the enclosed integrated system, which does not allow the DGS to radiate and resonate at the designed frequency. For an embedded component, using a DGS in an inner layer can excite cavity resonances and cause EMI issues for other components found in inner layers. The issues due to radiation can be resolved

by using a resonant ground structure instead of a DGS for enclosed and embedded microwave components.

4.2 Resonant Ground Structure Theory

A recent derivative of DGS technology is the resonant ground structure (RGS) that contains radiated fields from the defect in a dielectric substrate [38]. Resonant ground structures provide significant signal suppression for embedded and enclosed microstrip components. All the radiated fields are captured inside a dielectric substrate that keeps radiation from affecting other systems or components. The resonant ground structure first proposed in [38] has a substrate-filled metallic cavity as shown in Fig. 4.3. The resonant ground structure proposed in this work uses a tightly-spaced via cage to enclose the radiated fields of the defect in the ground structure. This new resonant ground structure is planar, easy to fabricate, and useful for inner layers.

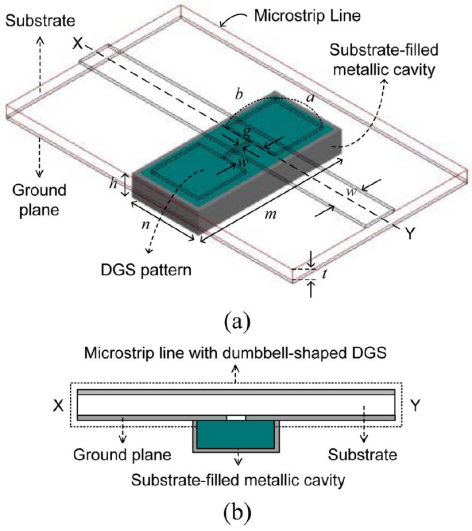

Figure 4.3: Isometric View (a) and Side View (b) of Barbell RGS in Microstrip [38]

4.3 Design Parameters

A resonant ground structure is simulated in HFSS using a SISL cavity model with a suspended thru-line as shown in Fig 4.4. This is done to easily study the design parameters of the RGS. The dielectric substrate has a different permittivity than air and finite thickness. These differences add two extra design parameters to consider when designing an RGS as shown in Fig. 4.5.

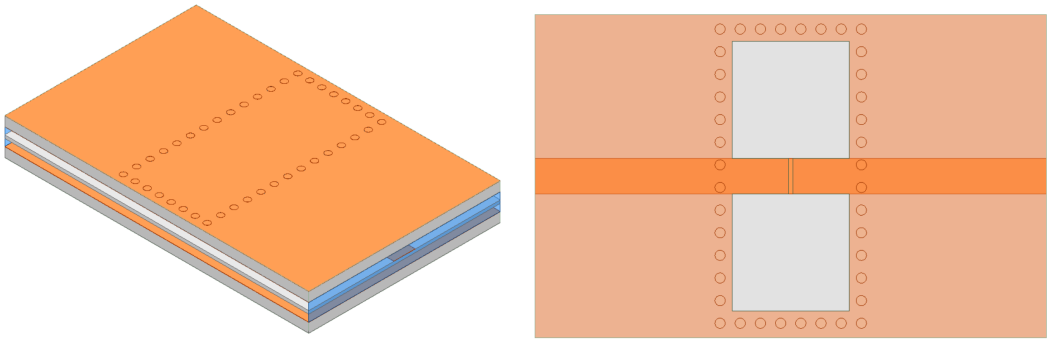

(a) Isometric View (b) Top View

Figure 4.4: RGS Cavity Model

Figure 4.5: Substrate Dimensions of the RGS

The first extra design parameter studied in this work is the permittivity of the dielectric substrate. Keeping all the dimensions of the defect in the ground plane the same, the permittivity was varied to observe the change in resonant frequency and 10 dB percent bandwidth. The general trend with varying the permittivity of the substrate is that a higher permittivity decreases the resonant frequency and the percent bandwidth (see Fig. 4.6 and Table 4.1). This behavior is because increas-

ing permittivity increases the capacitance of the structure. Based on the equations of the equivalent LC model, increasing the capacitance will decrease the resonant frequency and the bandwidth. Substrates with high loss tangents will also reduce the percent bandwidth of the notch filter.

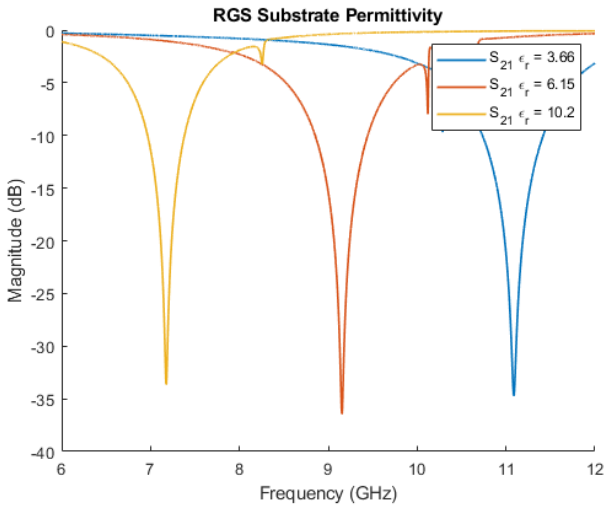

Figure 4.6: Transmission Behaviour of Varied Permittivity in RGS Substrate

Class	ϵ_r = 3.66	ϵ_r = 6.15	ϵ_r = 10.2
Loss Tangent	0.004	0.0019	0.0023
Resonant Frequency (GHz)	11.09	9.15	7.18
Percent Bandwidth (10 dB)	6.1 %	6.5 %	5.7 %

Table 4.1: Metrics of Varied Permittivity

The second extra design parameter studied in this work is the thickness of the dielectric substrate. Again, keeping all the dimensions of the defect in the ground plane the same, the thickness of the substrate was varied to observe the change in resonant frequency and 10 dB percent bandwidth. The general trend with varying the thickness of the dielectric substrate is that a thicker dielectric substrate decreases

the resonant frequency and increases the percent bandwidth of the notch filter (see Fig. 4.7 and Table 4.2). This behavior is because increasing thickness increases the inductance of the structure. Based on the equations of the equivalent LC model, increasing the inductance will decrease the resonant frequency and increase the bandwidth.

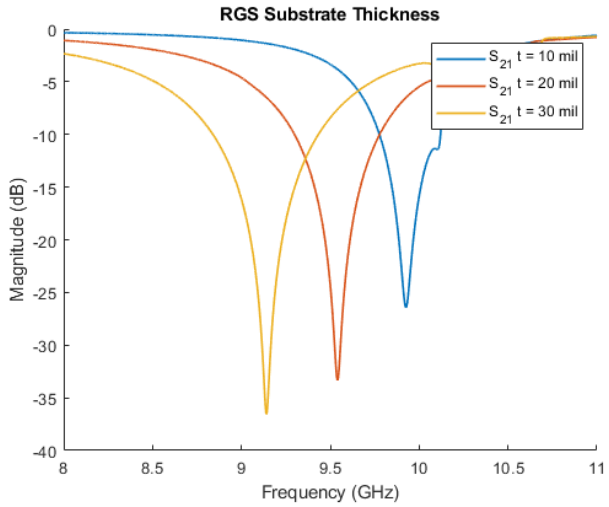

Figure 4.7: Transmission Behaviour of Varied Thickness in RGS Substrate

Class	t = 10 mil	t = 20 mil	t = 30 mil
Resonant Frequency (GHz)	9.93	9.54	9.14
Percent Bandwidth (10 dB)	3.4 %	5.0 %	6.5 %

Table 4.2: Metrics of Varied Thickness

4.4 Design Steps

Using the parameter study above, a design process is developed for creating resonant ground structures for spurious suppression. First, a substrate with desirable permittivity and thickness must be chosen for a reasonable resonant frequency and

suppression level. Higher permittivity substrates allow for smaller RGSs to save valuable board space but have less suppression bandwidth. Lower permittivity substrates have more suppression bandwidth but increase the size of the RGS. Next, the dimensions of the RGS need to be estimated for the desired resonant frequency based on the equivalent inductance and capacitance. No design equations exist for RGSs, so designers must estimate the dimensions for the correct resonant frequency. The design is then simulated with the calculated dimensions of the RGS to verify the desired resonant frequency. The dimensions of the RGS are then altered by changing the size of the barbell ends or the distance of the center gap to account for estimation error. A design flow graph of the process in shown in Fig. 4.8.

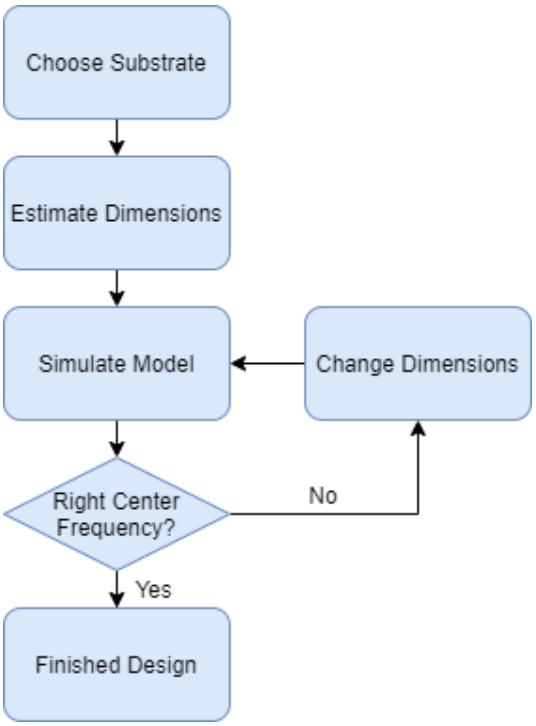

Figure 4.8: RGS Design Flow Graph

4.5 Simulated Results

After the RGSs have been designed to the correct center frequency, they can be placed on the input of the filter to test the signal suppression. An RGS is simulated for suppressing the spurious responses at 8 and 10 GHz, and the cavity resonance at 9.14 GHz in the HFSS model shown in Fig. 4.9. Again, the cavity filter model was used for simulation to cut down on simulation time.

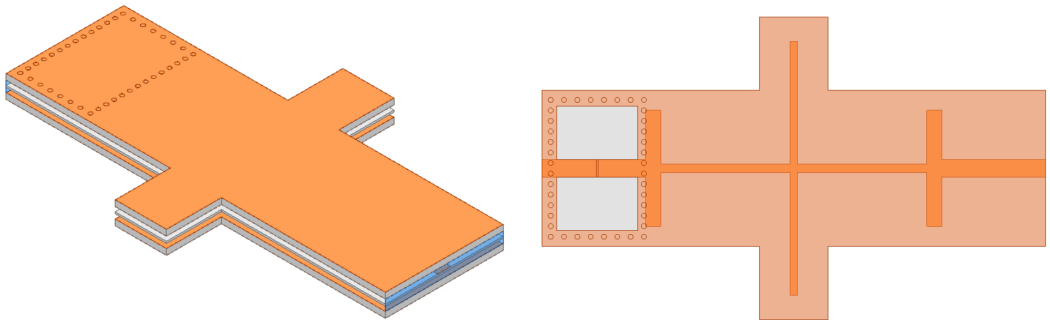

(a) Isometric View (b) Top View

Figure 4.9: RGS Cavity Filter Model

An RGS was designed to resonate at 8 GHz to suppress the first spurious response of the filter. The RGS fully suppresses the first spurious response of the filter as shown in Fig. 4.10. The 8 GHz RGS greatly suppresses the spurious response well below the -10 dB goal level of S_{21} to at least -11 dB for the entire spurious response. Similar to the aperture coupled SIW resonators, S_{11} is marginally increased in the passband of the filter. At this frequency, the bandwidth of the RGS is large enough to suppress the spurious response.

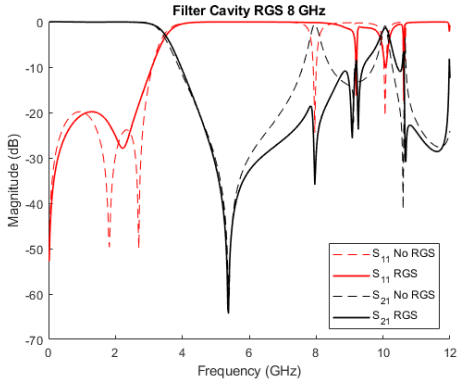

(a) Filter Response

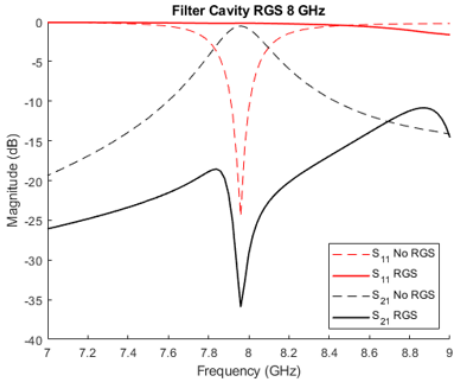

(b) Spurious Suppression

Figure 4.10: Cavity Filter with RGS at 8 GHz

Next, an RGS resonator was designed to resonate at 10 GHz to suppress the second spurious response of the filter. This RGS only partially suppresses the second spurious response of the filter below the goal level as shown in Fig. 4.11. The RGS at 10 GHz suppresses the spurious response to only -4 dB in S_{21}. At this frequency, the RGS does not have enough suppression bandwidth to suppress the entire spurious response.

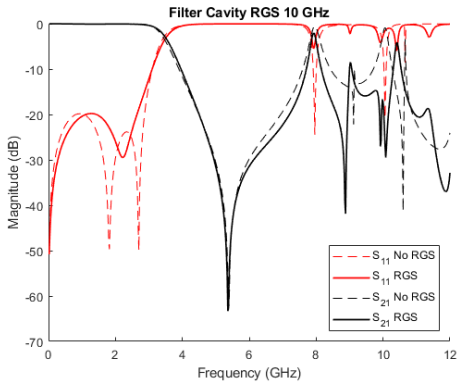

(a) Filter Response

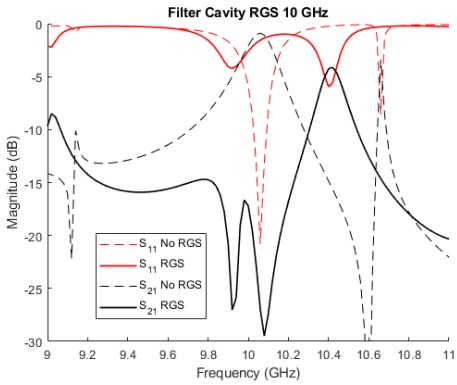

(b) Spurious Suppression

Figure 4.11: Cavity Filter with RGS at 10 GHz

Lastly, an RGS was designed to resonate at 9.14 GHz to dampen the first spurious cavity resonance of the filter. The RGS does not dampen the spur caused by the

cavity resonance as shown in Fig. 6.1. The RGS does not dampen the unintentional resonance because it behaves fundamentally differently than the aperture coupled SIW resonator. The RGS does not magnetically couple through the magnetic fields of the excited cavity resonance, so the RGS is not capable of dampening the cavity resonance.

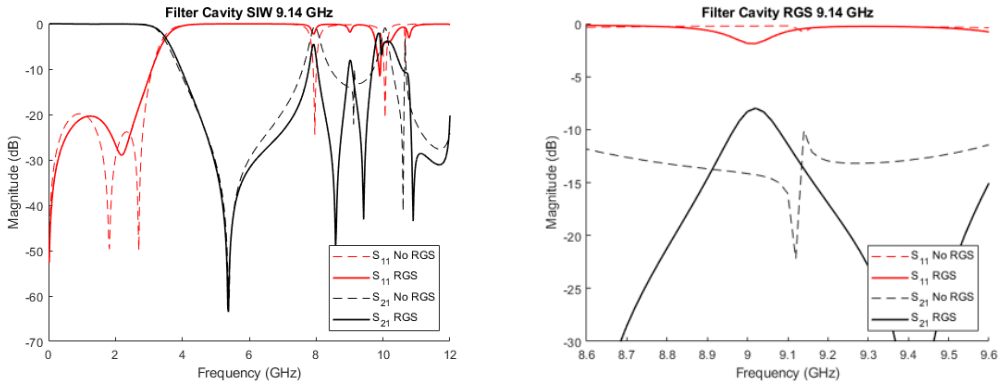

(a) Filter Response (b) Spurious Suppression

Figure 4.12: Cavity Filter with RGS at 9.14 GHz

4.6 Conclusions

The resonant ground structures suppress the spurious responses better than the aperture coupled SIW resonators. Compared to aperture coupled SIW resonators, RGSs take longer to design because there are no design equations that define them, so the design must be simulated iteratively until the center frequency is correct. Resonant ground structures provide adequate suppression for the commensurate line filter but do not dampen the cavity resonances of the filter. The initial design and simulation in this chapter are verified in the following chapter by fabricating and measuring the SISL filter with RGSs in the ground plane as a spurious suppression technique.

Chapter 5

Results and Analysis

This chapter details the fabrication and measured results for the resonant ground structures in the SISL filter designed in Chapter 2. The measured results of the filter are analyzed to provide insight into resonant ground structures and their overall effect on filter performance.

5.1 Fabrication

This section outlines the steps to fabricate the SISL filter with the resonant ground structures. The LPFK ProtoLaser U4 was used in the fabrication process to laser etch and cut the board material. LPKF ProConduct was used to plate the vias for the CPWG, SISL via cage, and RGS via cage. Screws and nuts were used to keep the board layers together. Appendix A has more detailed step-by-step instructions. Below are the basic steps in the fabrication process of the SISL filter.

Fabrication Steps:

1. Generate Gerber files
2. Laser etch the board design
3. Mill vias with the milling machine

4. Plate vias with ProConduct

5. Laser cut screw holes and cavities

6. Solder on the edge-launch connectors

7. Screw layers together

These steps were followed to fabricate the filter shown in Fig. 5.1. The top and bottom substrates can easily be rotated to have the ground plane with or without an RGS. The top and bottom substrates are rotated to test the RGSs individually and together.

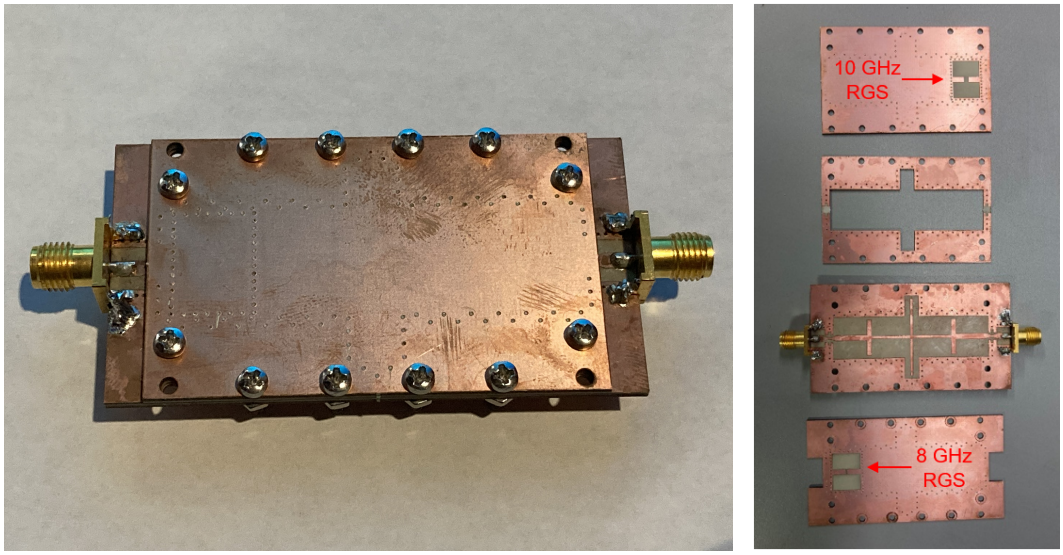

(a) Assembled SISL Filter (b) Board Stack Up

Figure 5.1: Fabricated SISL Filter

5.2 Measured Results

The SISL filter was measured to test the resonant ground structures on the top and bottom ground planes that suppressed the spurious responses at 8 and 10 GHz. To acknowledge that the RGS works as expected, a SISL thru-line is tested with

and without the 8 and 10 GHz RGS on the bottom substrate. The responses of the thru-line with the RGS are shown in Fig. 5.2 below.

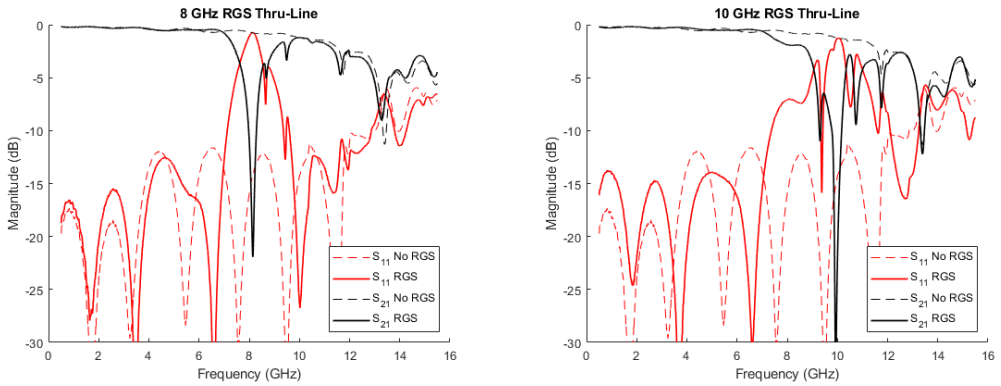

(a) 8 GHz RGS Response (b) 10 GHz RGS Response

Figure 5.2: S-Parameters of RGSs in SISL Thru-line

The RGSs were then measured together on opposite ground planes on the input of the filter to show that the RGSs behave independently of each other. Cavity resonances from the via cages distort the response of the RGSs in the stopband, but these can be ignored because they provide extra suppression in the stopband.

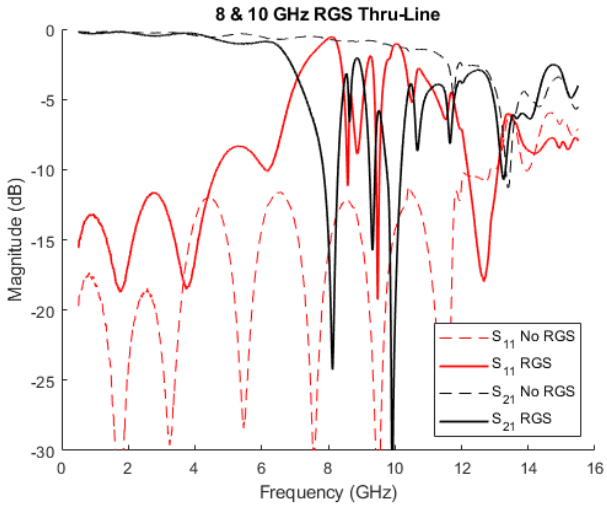

Figure 5.3: S-Parameters of RGSs in SISL Thru-line

The first RGS tested was on the bottom ground plane and suppressed the spurious response at 8 GHz. The RGS on the bottom ground plane was tested on both the input and output of the filter and was shown to have a similar filter response. The RGS on the bottom substrate suppressed the spurious response to below 6 dB and increased the peak return loss of the filter in the passband to 18 dB.

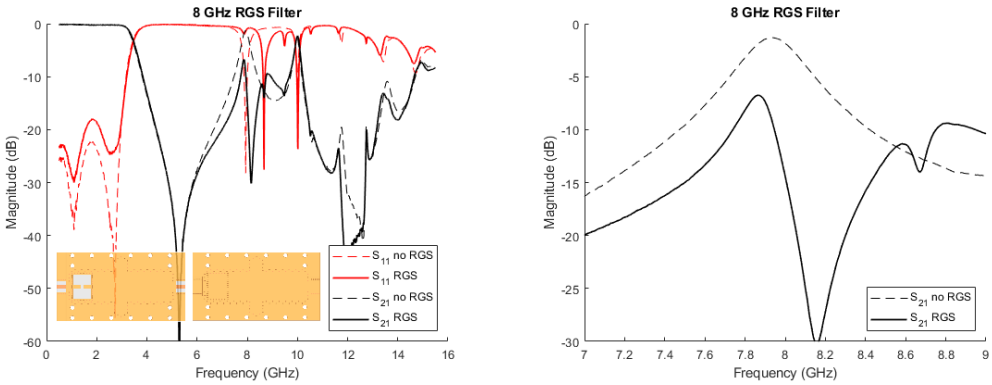

(a) Filter Response (b) Spurious Suppression

Figure 5.4: Responses of 8 GHz RGS in SISL Filter

The second RGS tested was on the top ground plane and suppressed the spurious response at 10 GHz. The RGS on the top ground plane was tested on both the input and output of the filter and was shown to have a similar filter response. The RGS on the bottom substrate suppressed the spurious response to below 8 dB and increased the peak return loss of the filter in the passband to 17 dB.

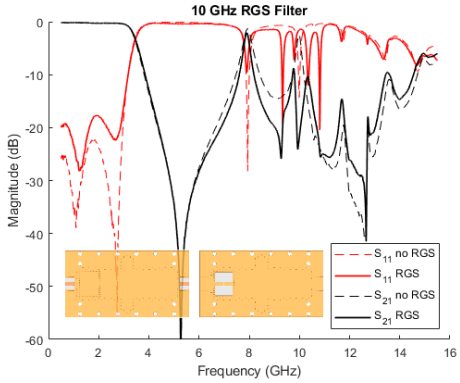

(a) Filter Response

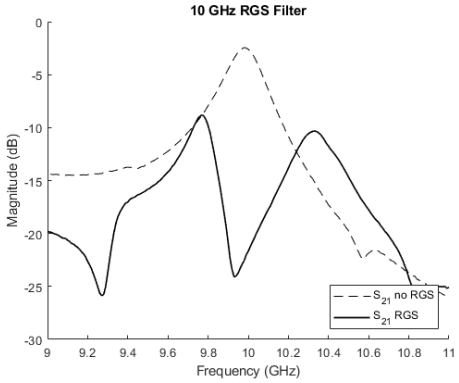

(b) Spurious Suppression

Figure 5.5: Responses of 10 GHz RGS in SISL Filter

The last configuration tested used both RGSs on the top and bottom ground plane to suppress the spurious responses at 8 and 10 GHz. All the variations of placing the RGSs on the input and output of the filter were shown to have similar responses. Together, the RGSs on the top and bottom ground plane suppressed the spurious responses to below 10 dB and increased the peak return loss of the filter in the passband to 13 dB.

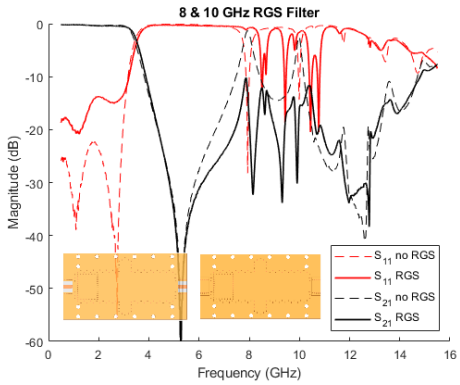

(a) Filter Response

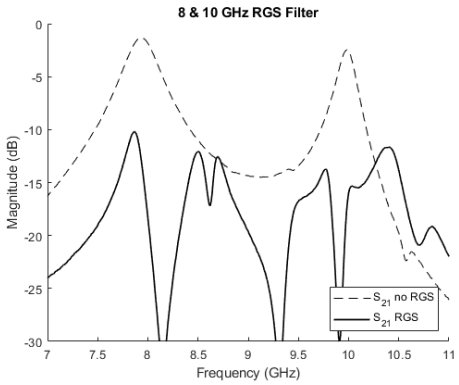

(b) Spurious Suppression

Figure 5.6: Responses of 8 and 10 GHz RGS in SISL Filter

5.3 Analysis

Together, the resonant ground structures suppress the spurious responses of the filter below 10 dB up to 14.5 GHz. This means that spurious signals at frequencies below 14.5 GHz going through the filter will be attenuated to less than 10% of their original signal strength. However, the introduction of the RGSs increases the cutoff frequency by 100 MHz and decreases the return loss in the passband by 8 dB. This is because RGSs create defects in the ground plane which induces extra inductances and capacitances on the input commensurate line. The induced capacitances and inductances change the characteristic impedance of the input line to the filter from 50-ohm. A different characteristic impedance from the 50-ohm system causes an impedance mismatch that increases the return loss in the passband and the cutoff frequency. The input line of the filter was simulated separately in HFSS and was shown to have a characteristic impedance of 49 ohms in the center of the passband at 1.5 GHz The input line of the filter was then simulated with the two RGSs used in the fabricated filter and was shown to have a characteristic impedance of 48 ohms at 1.5 GHz. Advanced Design Software (ADS) was used to verify that the mismatch from 49 to 48 ohms would cause a decrease in return loss comparable to that seen in the measured filter. ADS showed a decrease in return loss by a little over 5 dB from the 49-ohm to the 48-ohm line. The extra 3 dB of decreased return loss can be accounted for by dielectric and leakage losses of the RGS substrate and via cage, respectively. The major mismatch effect on the input line of the filter can be compensated for by reducing the width of the input line to achieve a better 50-ohm match in the passband.

Chapter 6

Conclusion

The purpose of this chapter is to summarize the work, note its scientific impact, and suggest areas of future work. The chapter summarizes the important findings in aperture coupled SIW resonators and resonant ground structures for suppressing spurious signals. The findings of this work have broad implications for microwave component design in integrated and embedded applications. There are many more areas that can be explored to suppress the spurious signals of microwave components.

6.1 Summary

This work explored two different techniques to suppress the spurious responses of an embedded microwave filter. The spurious responses happen due to the standing wave effects of the commensurate line and the cavity resonances of the via cage surrounding the filter. Aperture coupled SIW resonators were the first technique of spurious suppression explored because of their intuitive and well-defined design. It has been shown in simulation that aperture coupled SIW resonators can dampen the cavity resonances in the embedded filter by absorbing the energy in its dielectric. However, aperture coupled SIW resonators did not have the band-

width to adequately suppress the spurious responses due to the commensurate line filter, only suppressing the responses by 1 to 3 dB. The second technique of spurious suppression explored in this work is resonant ground structures. Even though resonant ground structures have a more difficult design, they provide adequate suppression of over 10 dB for the spurious responses caused by the commensurate line filter as shown in simulated and measured results. The resonant ground structures, however, did not dampen the cavity resonances of the via cage like the aperture coupled SIW resonators. Both of the techniques explored in this study have defects in the ground plane that induce inductances and capacitances on the commensurate line that changes the characteristic impedance and causes more reflection due to mismatch.

6.2 Scientific Impact

The two techniques of spurious suppression discussed in this work will enhance the performance of integrated and embedded microwave components. For RF front ends, these techniques can reduce the number of high power spurious signals received that damage sensitive components and alter data. For RF back ends, this technology can reduce the number of spurious signals transmitted that waste transmit power and interfere with other RF systems. The spurious suppression techniques explored can be used in many different integrated microwave components such as antennas, amplifiers, mixers, and power dividers without changing the inherent geometry or causing radiation issues. The techniques explored in this work allow for easy design and implementation of spurious suppression in existing microwave components and systems.

6.3 Future Work

There are many other areas of spurious suppression that can be explored in future work. This section suggests areas of exploration in integrated and embedded microwave components.

6.3.1 Absorptive Filter

Aperture coupled SIW resonators have the potential to absorb the cavity resonances found in many integrated and embedded filter applications. Resonators are the building blocks to filters, so multiple SIW resonators can potentially be coupled together to form an absorptive filter on top of the embedded filter designed in this work. Previous research has demonstrated an absorptive 2nd order Butterworth bandstop filter in microstrip using SIW resonators as shown in Fig. 6.1a [39, 40]. A similar structure can be designed in one of the sacrificial ground planes to absorb the cavity resonances of the embedded filter. Preliminary research was done to simulate an absorptive filter in SISL, and its response is shown in Fig. 6.1b. An absorptive filter creates a null in both S_{11} and S_{21} since signals are neither reflected or transmitted, but absorbed.

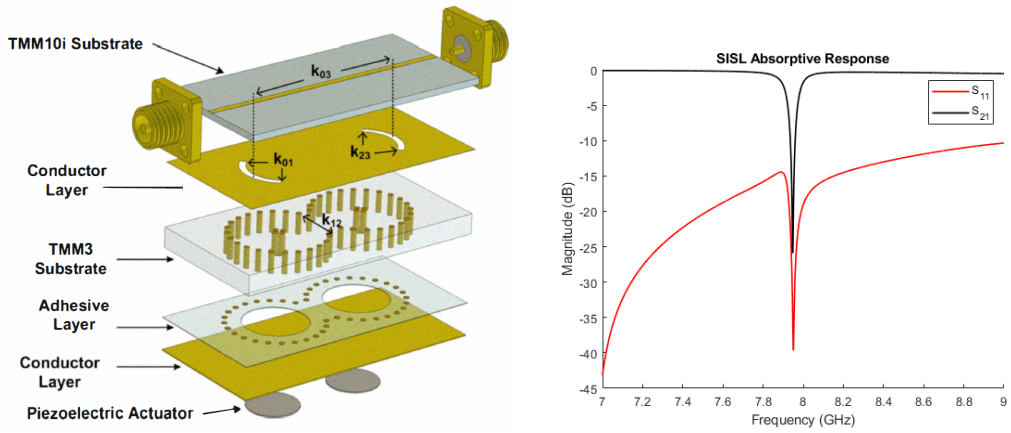

(a) Exploded View of Absorptive Filter [39] (b) Absorptive Response in SISL Thru-line

Figure 6.1: Absorptive Filter Response in SISL

6.3.2 RGS Design Equations

The resonant ground structures designed using the cavity models in this work were simulated many times before achieving the desirable behavior. Creating accurate design equations to model the resonant ground structure for a simple barbell would cut down on the number of simulations and reduce design time. Modeling the resonant ground structures as a parallel RLC circuit would enhance the understanding of the RGS from a circuits perspective. An accurate equivalent model has yet to be created for defected ground structures. Resonant ground structures add design parameters due to the thickness and permittivity of the substrate. Creating an equivalent circuit model of an RGS would require extensive curve-fitting, which would involve simulating the RGS model many times and slightly varying the design parameters each time. With at least 8 design variables necessary to characterize an RGS, this would be a time-intensive process and is beyond the scope of this research.

6.3.3 Coplanar RGSs

Another avenue for future work is characterizing the behavior of two or more resonant ground structures on the same ground plane. Defected ground structures are often placed in series and can even be periodic across a transmission line. Designing and simulating coplanar resonant ground structures would increase understanding of how resonant ground structures behave together. Initial research shows that the responses of the RGSs are not independent of one another when on the same ground plane. An understanding of how RGSs behave on the same ground plane could help designers better suppress spurious signals and responses in microwave components.

6.3.4 Absorptive Vias

Absorptive material with high permittivity and permeability dampens cavity resonances in microwave applications. Absorber material is commonly coated on EMI shields to dampen cavity resonances for high-frequency circuits [5]. Adding absorber material on the outside of the SISL air cavity would change the effective permittivity of the cavity, and thus change the response of the embedded filter. A recent study shows that only coating the outer edges of the cavity dampens the cavity resonances of a parallel plate structure by absorbing the magnetic currents along the sidewalls [41]. For integrated applications, absorptive material could be deposited in vias around the SISL air cavity much like how the ProConduct was applied to the unplated vias in fabrication. This solution has the potential to dampen the cavity resonances of the embedded filter without changing the effective permittivity of the air cavity.

References

[1] G. Ludeno, I. Catapano, A. Renga, A. R. Vetrella, G. Fasano, and F. Soldovieri, "Assessment of a micro-uav system for microwave tomography radar imaging," *Remote Sensing of Environment*, vol. 212, pp. 90–102, 2018. [Online]. Available: https://www.sciencedirect.com/science/article/pii/S0034425718301974

[2] K. K. Samanta and D. Kissinger, "Multilayer millimeter-wave mcms [from the guest editors' desk]," *IEEE Microwave Magazine*, vol. 19, no. 1, pp. 20–135, 2018.

[3] N. Microwave-East. [Online]. Available: https://www.rfglobalnet.com/doc/integrated-microwave-assembly-ima-0002

[4] D. M. Pozar, *Microwave engineering; 3rd ed.* Hoboken, NJ: Wiley, 2005. [Online]. Available: https://cds.cern.ch/record/882338

[5] P. Dixon, "Dampening cavity resonance using absorber material," *RF Design Magazine*, pp. 16–19, 2004.

[6] "Distributed-element circuit," Jun 2021. [Online]. Available: https://en.wikipedia.org/wiki/Distributed-element_circuit

[7] M. S. Parihar, A. Basu, and S. K. Koul, "Efficient spurious rejection and null steering using slot antennas," *IEEE Antennas and Wireless Propagation Letters*, vol. 10, pp. 207–210, 2011.

[8] A. Kiayani, L. Anttila, and M. Valkama, "Digital suppression of power amplifier spurious emissions at receiver band in fdd transceivers," *IEEE Signal Processing Letters*, vol. 21, no. 1, pp. 69–73, 2014.

[9] S. A. Kosmopoulos and C. Cornacchini, "Spurious-response suppression evaluation of space qualified millimeter wave mixers: A distributed and parasitic effects approach," *International Journal of Infrared and Millimeter Waves*, vol. 13, no. 2, pp. 197–206, Feb. 1992.

[10] J.-T. Kuo, J.-S. Wu, and Y.-C. Chiou, "Miniaturized rat race coupler with suppression of spurious passband," *IEEE Microwave and Wireless Components Letters*, vol. 17, no. 1, pp. 46–48, 2007.

[11] P. Cheong, S.-W. Fok, and K.-W. Tam, "Miniaturized parallel coupled-line bandpass filter with spurious-response suppression," *IEEE Transactions on Microwave Theory and Techniques*, vol. 53, no. 5, pp. 1810–1816, 2005.

[12] M. Salehi and E. Mehrshahi, "Spurious-response suppression of substrate integrated waveguide filters using multishape resonators and slotted plane structures," *International Journal of RF and Microwave Computer-Aided Engineering*, vol. 21, no. 6, pp. 650–657, 2011. [Online]. Available: https://onlinelibrary.wiley.com/doi/abs/10.1002/mmce.20560

[13] F. Karshenas, A. R. Mallahzadeh, and J. Rashed-Mohassel, "Size reduction and harmonic suppression of parallel coupled-line bandpass filters using defected ground structure," in *2009 13th International Symposium on Antenna Technology and Applied Electromagnetics and the Canadian Radio Science Meeting*, 2009, pp. 1–6.

[14] G. Breed, "An introduction to defected ground structures in microstrip circuits," *High Frequency Electronics*, vol. 7, 01 2008.

[15] L. G. Maloratsky, "Reviewing the basics of suspended striplines," *Microwave Journal*, Oct. 2002.

[16] N. Lioutas, "Design of Generalised Chebyshev Suspended Stripline Filters," Department of Defence, Defence Science and Technology Organization, Tech. Rep., 04 1986.

[17] R. Barrett, "Microwave printed circuits - the early years," *IEEE Transactions on Microwave Theory and Techniques*, vol. 32, no. 9, pp. 983–990, 1984.

[18] J. McDaniel, "Self-packaged and low-loss suspended integrated stripline filters for next generation systems," Ph.D. dissertation, University of Oklahoma, 2018.

[19] L. Li, K. Ma, N. Yan, Y. Wang, and S. Mou, "A novel transition from substrate integrated suspended line to conductor backed cpw," *IEEE Microwave and Wireless Components Letters*, vol. 26, no. 6, pp. 389–391, 2016.

[20] J. W. McDaniel, S. Saeedi, M. B. Yeary, and H. H. Sigmarsson, "A low-loss fully board-integrated low-pass filter using suspended integrated strip-line technology," *IEEE Transactions on Components, Packaging and Manufacturing Technology*, vol. 8, no. 11, pp. 1948–1955, 2018.

[21] J. McDaniel, S. Saeedi, and H. Sigmarsson, "A fully-board integrated ka-band suspended integrated strip-line thru and low pass filter," 03 2018.

[22] J. McDaniel and H. Sigmarsson, "Low-loss and ultra-wide passband highpass filter using suspended integrated strip-line technology," *Electronics Letters*, vol. 55, 05 2019.

[23] Z. Ma, K. Ma, S. Mou, and F. Meng, "Quasi-lumped-element filter based on substrate-integrated suspended line technology," *IEEE Transactions on Microwave Theory and Techniques*, vol. 65, no. 12, pp. 5154–5161, 2017.

[24] Y. Chen, K. Ma, and Y. Wang, "A ka-band substrate integrated suspended line to rectangular waveguide transition," *IEEE Microwave and Wireless Components Letters*, vol. 28, no. 9, pp. 744–746, 2018.

[25] L. Li, K. Ma, and S. Mou, "A novel high q inductor based on double-sided substrate integrated suspended line technology with patterned substrate," in *2017 IEEE MTT-S International Microwave Symposium (IMS)*, 2017, pp. 480–482.

[26] S. A. Alseyab, "A novel class of generalized chebyshev low-pass prototype for suspended substrate stripline filters," *IEEE Transactions on Microwave Theory and Techniques*, vol. 30, no. 9, pp. 1341–1347, 1982.

[27] J. W. McDaniel, "Simulation guidelines for wideband ground backed coplanar waveguide transmission lines," in *2019 IEEE 20th Wireless and Microwave Technology Conference (WAMICON)*, 2019, pp. 1–5.

[28] K. Wu, D. Deslandes, and Y. Cassivi, "The substrate integrated circuits - a new concept for high-frequency electronics and optoelectronics," in *6th International Conference on Telecommunications in Modern Satellite, Cable and Broadcasting Service, 2003. TELSIKS 2003.*, vol. 1, 2003, pp. P–III.

[29] X.-P. Chen and K. Wu, "Substrate integrated waveguide filter: Basic design rules and fundamental structure features," *IEEE Microwave Magazine*, vol. 15, no. 5, pp. 108–116, 2014.

[30] J. Rossello, F. Mira, A. Collado, and A. Georgiadis, "Substrate integrated waveguide aperture coupled patch antenna array for 24 ghz wireless backhaul and radar applications," in *2014 IEEE Conference on Antenna Measurements Applications (CAMA)*, 2014, pp. 1–2.

[31] T. Zhang, L. Li, Z. Zhu, and T. J. Cui, "A broadband planar balun using aperture-coupled microstrip-to-siw transition," *IEEE Microwave and Wireless Components Letters*, vol. 29, no. 8, pp. 532–534, 2019.

[32] F. Xu and K. Wu, "Guided-wave and leakage characteristics of substrate integrated waveguide," *IEEE Transactions on Microwave Theory and Techniques*, vol. 53, no. 1, pp. 66–73, 2005.

[33] I. Chang and B. Lee, "Design of defected ground structures for harmonic control of active microstrip antenna," in *IEEE Antennas and Propagation Society International Symposium (IEEE Cat. No.02CH37313)*, vol. 2, 2002, pp. 852–855 vol.2.

[34] J.-S. Lim, S.-W. Lee, C.-S. Kim, J.-S. Park, D. Ahn, and S. Nam, "A 4.1 unequal wilkinson power divider," *IEEE Microwave and Wireless Components Letters*, vol. 11, no. 3, pp. 124–126, 2001.

[35] C.-S. Kim, J.-S. Lim, J.-S. Park, D. Ahn, and S. Nam, "A 10db branch line coupler using defected ground structure," in *2000 30th European Microwave Conference*, 2000, pp. 1–4.

[36] D. Ahn, J.-S. Park, C.-S. Kim, J. Kim, Y. Qian, and T. Itoh, "A design of the low-pass filter using the novel microstrip defected ground structure," *IEEE Transactions on Microwave Theory and Techniques*, vol. 49, no. 1, pp. 86–93, 2001.

[37] C.-S. Kim, J.-S. Park, D. Ahn, and J.-B. Lim, "A novel 1-d periodic defected ground structure for planar circuits," *IEEE Microwave and Guided Wave Letters*, vol. 10, no. 4, pp. 131–133, 2000.

[38] I. Shin, T.-H. Lee, J. Lee, and Y.-S. Kim, "A novel resonant ground structure based on a cavity-backed dgs," *IEEE Microwave and Wireless Components Letters*, vol. 24, no. 5, pp. 321–323, 2014.

[39] T. Snow, J. Lee, and W. J. Chappell, "Tunable high quality-factor absorptive bandstop filter design," in *2012 IEEE/MTT-S International Microwave Symposium Digest*, 2012, pp. 1–3.

[40] J. Lee, E. J. Naglich, and W. J. Chappell, "Frequency response control in frequency-tunable bandstop filters," *IEEE Microwave and Wireless Components Letters*, vol. 20, no. 12, pp. 669–671, 2010.

[41] S. Huang, G. Charles, K. Xiao, B. Lee, G. Ouyang, and H. Zhang, "Suppression of cavity resonant edge effects and pdn impedance using absorbing material," in *2015 IEEE Symposium on Electromagnetic Compatibility and Signal Integrity*, 2015, pp. 12–16.

[42] LPKF, "LPKF ProtoLaser U4," Accessed on 2021-06-17. [Online]. Available: https://www.lpkf.com/en/industries-technologies/research-in-house-pcb-prototyping/produkte/lpkf-protolaser-u4

[43] ——, “LPKF ProtoMat S103,” Accessed on 2021-21-17. [Online]. Available: https://www.lpkfusa.com/datasheets/prototyping/s103.pdf

[44] ——, “ProConduct,” Accessed on 2021-06-17. [Online]. Available: https://www.lpkfusa.com/products/pcb_prototyping/through-hole_plating_and_multilayer/proconduct/

Appendix A

SISL Filter Fabrication Process

The purpose of this appendix is to document a detailed fabrication process for the SISL filter designed in this work. All of the drilling steps can completed using an LPKF ProtoLaser U4 milling machine [42], but a drill milling machine was used to mill out the vias [43]. For the SISL filter build, there are 15 Gerber files generated that are needed to fabricate the design. The required Gerber files are as follows:

1. Copper_Layer_1 - metal layer 1 (M1)
2. Copper_Layer_2 - metal layer 2 (M2)
3. Copper_Layer_3 - metal layer 3 (M3)
4. Copper_Layer_4 - metal layer 4 (M4)
5. Copper_Layer_5 - metal layer 5 (M5)
6. Copper_Layer_6 - metal layer 6 (M6)
7. Copper_Layer_7 - metal layer 7 (M7)
8. Copper_Layer_8 - metal layer 8 (M8)
9. Copper_Layer_9 - metal layer 9 (M9)

10. Copper_Layer_10 - metal layer 10 (M10)

11. Substrate_Cutout - gerber file used to cut out air cavity

12. Screwholes - ncd drill file used to drill out screwholes

13. Via_Cage - ncd drill file used to drill via cage for the SISL cavity and CPWG

14. RGS_Top - ncd drill file used to drill the via cage for the top RGS

15. RGS_Bottom - ncd drill file used to drill the via cage for the bottom RGS

16. Fiducials - ncd drill file used to align the laser machine

A.1 Detailed Fabrication Process

The fabrication process is broken down into 4 steps as follows:

1. Laser Etch Board Design

2. ProConduct Process

3. Laser Cut Board Design

4. Assemble Layers

A.1.1 Laser Etch Board Designs

For each substrate, the board designs are etched first in the fabrication process. This is done before plating the vias because the adhesive used in the ProConduct process can interfere with the laser etching. Fiducials need to be cut out for each layer to align the laser machine for etching both sides of the board and for later fabrication steps.

A.1.2 ProConduct Process

ProConduct is a process to plate vias for rapid prototyping of in-house board designs [44]. The steps for the ProConduct process to plate the vias are as follows:

1. Apply the protective film to both sides of etched board design
2. Remove protective film around fiducial holes for protolaser to read them
3. Laser cut all the vias for each board laser
4. Apply the conductive polymer to the PCB and squeegee over the surface to fill the vias
5. Use the vacuum table to remove the excess conductor
6. Repeat steps 4 and 5 for the other side of the board
7. Remove the protective film from the board
8. Cure the polymer in a hot-air oven for 30 minutes at 160° C.
9. Clean the board with the LPKF cleaning solution

A.1.3 Laser Cut Board Designs

After the ProConduct process is complete, the board designs need to be laser cut. Screwholes are cut from all the boards to fix them together and provide sufficient electrical connection and enclosure of the air cavity. The cavities are cut from substrates 2 and 4 to suspend the stripline in air. Lastly, the board outline is cut out from each substrate so that the board can be connected via edge launch connectors.

A.1.4 Assemble Layers

After the layers are laser cut, they need to be assembled together to be tested. The first step in assembling the design for testing is to solder edge launch connectors on both the input and output of the filter for substrates 3 and 4. Next, all the layers need to be bolted together with screws and nuts. The resonant ground structures can be in any desired orientation for this step. The screws need to be tight to ensure sufficient electrical connection between layers and a fully enclosed SISL cavity.

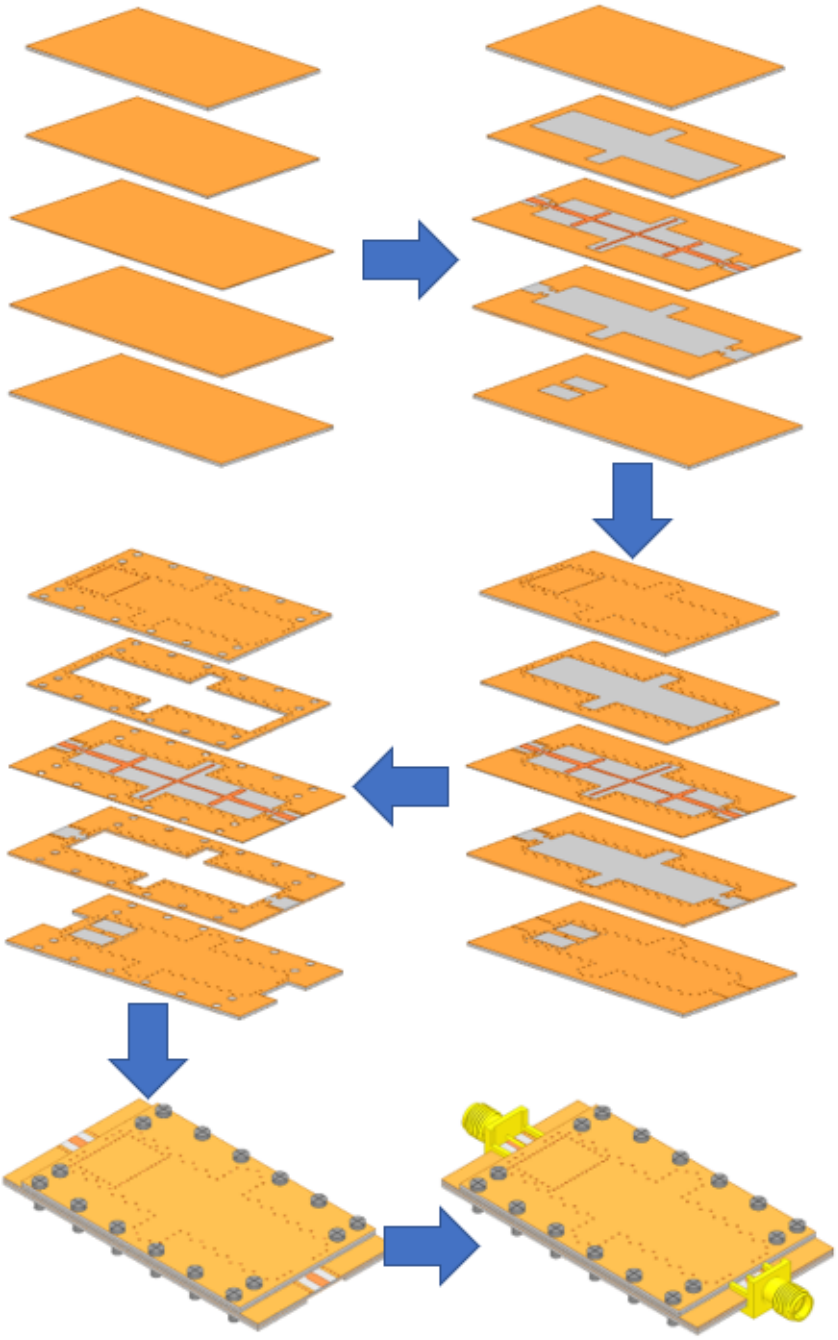

Figure A.1: Fabrication Process of SISL Filter

Appendix B

List of Acronyms and Abbreviations

ADS Advanced Design Software

CPWG Coplanar Waveguide Grounded

DGS Defected Ground Structure

EMC Electromagnetic Compatibility

EMI Electromagnetic Interference

EM Electromagnetic

HFSS High Frequency Structure Simulator

HOM Higher-Order Mode

IMA Integrated Microwave Assemblies

LPF Low-Pass Filter

MCM Multi-chip Module

MWO Microwave Office

PCB Printed Circuit Board

RF Radio Frequency

RGS Resonant Ground Structure

Rx Receive

SISL Suspended Integrated Stripline

SIW Substrate Integrated Waveguide

SWaP-C Size, Weight, Power, and Cost

Tx Transmit

UAV Unmanned Aerial Vehicle